NIH Public Access
Author Manuscript
Neuroimage. Author manuscript; available in PMC 2014 August 09.

Published in final edited form as:
Neuroimage. 2013 April 15; 70: 340–355. doi:10.1016/j.neuroimage.2012.12.031.

The Structural Connectome of the Human Brain in Agenesis of the Corpus Callosum

Julia P. Owen[1,2], **Yi-Ou Li**[1], **Etay Ziv**[1], **Zoe Strominger**[3], **Jacquelyn Gold**[3], **Polina Bukhpun**[3], **Mari Wakahiro**[3], **Eric J. Friedman**[4], **Elliott H. Sherr**[3], and **Pratik Mukherjee**[*,1,2]

[1]Department of Radiology & Biomedical Imaging, University of California, San Francisco

[2]Department of Bioengineering & Therapeutic Sciences, University of California, San Francisco

[3]Department of Neurology, University of California, San Francisco

[4]International Computer Science Institute, University of California, Berkeley

Abstract

Adopting a network perspective, the structural connectome reveals the large-scale white matter connectivity of the human brain, yielding insights into cerebral organization otherwise inaccessible to researchers and clinicians. Connectomics has great potential for elucidating abnormal connectivity in congenital brain malformations, especially axonal pathfinding disorders. Agenesis of the corpus callosum (AgCC) is one of the most common brain malformations and can also be considered a prototypical genetic disorder of axonal guidance in humans. In this exploratory study, the structural connectome of AgCC is mapped and compared to that of the normal human brain. Multiple levels of granularity of the AgCC connectome are investigated, including summary network metrics, modularity analysis, and network consistency measures, with comparison to the normal structural connectome after simulated removal of all callosal connections ("virtual callostomy"). These investigations reveal four major findings. First, global connectivity is abnormally reduced in AgCC, but local connectivity is increased. Second, the network topology of AgCC is more variable than that of the normal human connectome, contradicting the predictions of the virtual callosotomy model. Third, modularity analysis reveals that many of the tracts that comprise the structural core of the cerebral cortex have relatively weak connectivity in AgCC, especially the cingulate bundles bilaterally. Finally, virtual lesions of the Probst bundles in the AgCC connectome demonstrate that there is consistency across subjects in many of the connections generated by these ectopic white matter tracts, and that they are a mixture of cortical and subcortical fibers. These results go beyond prior diffusion tractography studies to provide a systems-level perspective on anomalous connectivity in AgCC. Furthermore, this work

© 2014 Elsevier Inc. All rights reserved.

[*]Corresponding Author: Pratik Mukherjee, MD PhD, Center for Molecular and Functional Imaging, Department of Radiology and Biomedical Imaging, University of California, San Francisco, UCSF Box 0946, 185 Berry Street, Suite 350, San Francisco, CA 94107, pratik.mukherjee@ucsf.edu.

Publisher's Disclaimer: This is a PDF file of an unedited manuscript that has been accepted for publication. As a service to our customers we are providing this early version of the manuscript. The manuscript will undergo copyediting, typesetting, and review of the resulting proof before it is published in its final citable form. Please note that during the production process errors may be discovered which could affect the content, and all legal disclaimers that apply to the journal pertain.

NIH-PA Author Manuscript
NIH-PA Author Manuscript
NIH-PA Author Manuscript

NIH-PA Author Manuscript

NIH-PA Author Manuscript

NIH-PA Author Manuscript

offers a proof of principle for the utility of the connectome framework in neurodevelopmental disorders.

Keywords

structural connectivity; diffusion-weighted imaging; tractography; congenital brain malformation; brain development

Introduction

Recent advances in imaging technology, computational power and mathematical tools for network analysis have enabled the investigation of brain organization at the systems level, creating a new field of neuroscience known as “MR connectomics”. The structural connectome framework in particular provides a potent method for assessing the global white matter connectivity of the human brain (Sporns et al., 2005). The application of connectomics to healthy volunteers has elucidated the large-scale topology of the normal adult brain (Bullmore and Sporns, 2009; Gong et al., 2009; Hagmann et al, 2007; Hagmann et al., 2010; van den Heuvel and Sporns, 2011; Iturria-Medina et al., 2007; Li et al., 2012a,b; Sporns 2011). There are consistent findings across these publications, including the presence of highly connected brain regions, referred to as hubs. Building on this initial success, structural connectomics is now being applied to human brain development (Fan et al., 2011; Hagmann et al., 2012; Tymofiyeva et al., 2012; Yan et al., 2011; Yap et al., 2011) and to neurological and psychiatric disorders (Alscott et al., 2009; Irimia et al., 2012; Shu et al., 2009; Verstraete et al., 2011). Borrowing techniques from graph theory, summary metrics can be calculated to quantify key characteristics of the networks (Rubinov and Sporns, 2010). Community detection or modularity analysis has also been applied to the structural connectome to find groups of nodes that are strongly interconnected and therefore likely to be functionally integrated as well (Hagmann et al., 2008). These analysis methods reduce the dimensionality of the human connectome and enable statistical inferences to be more specific and better powered (Meskaldji et al., 2011).

The connectome framework is ideal for studying congenital brain malformations, especially disorders of axonal pathfinding leading to aberrant structural connectivity (Engle et al., 2010; Nugent et al., 2012, Wahl et al., 2010). Agenesis of the corpus callosum (AgCC) is one of the most common human brain malformations, occurring in at least 1 in 4000 live births (Glass et al., 2008; Wang et al., 2004) and in 3–5% of individuals assessed for neurodevelopmental disorders (Bodensteiner et al., 1994; Jeret et al., 1985). AgCC can also be considered a prototypical human disorder of axon guidance, one in which fibers that would normally have crossed the midline as part of the corpus callosum instead form Probst bundles, large white matter tracts that course anterior-posterior parallel to the interhemispheric fissure within each cerebral hemisphere (Paul et al., 2007; Paul et al., 2011). These gross anatomical abnormalities are easily diagnosed with conventional MRI, but macrostructural images may only scratch the surface of the extensive white matter reorganization in axonal pathfinding disorders. Diffusion MR tractography studies have shown some alterations of white matter connectivity in AgCC (Lee et al., 2004; Lee et al.,

NIH-PA Author Manuscript

NIH-PA Author Manuscript

NIH-PA Author Manuscript

2005; Tovar-Moll et al., 2007; Wahl et al., 2009; Nakata et al., 2009), but, to our knowledge, there has not been a systems-level investigation of connectivity in the acallosal brain. MR connectomics applied to AgCC may better characterize white matter abnormalities and potentially discover new anatomically subtle but functionally significant disruptions of connectivity that accompany this radiologically emblematic malformation. This could also serve as proof of principle for the utility of connectomics in more common neurodevelopmental disorders in which the underlying pathophysiological mechanism is also thought to be a "connectopathy", such as autism, dyslexia and schizophrenia (Seung 2012).

In this paper, multiple levels of granularity of the connectome are investigated. The most granular level is analyzing the individual edges of the graphs. Next, sets of edges or modules are tested for consistency and for statistical differences in connection strengths within the modules between the AgCC and control cohorts. At a larger scale, graph theoretic metrics such as degree are used to distinguish hub nodes from less-connected nodes. Finally, summary metrics, such as mean degree, characteristic path length and mean clustering coefficient, are used to characterize the entire network and provide tractable measures on which to perform statistics to compare whole connectomes.

These systems-level computational approaches are particularly powerful for exploring the importance of missing tracts or ectopic tracts, which are the hallmarks of axonal guidance disorders, through studying the effect of simulated lesions on the whole-brain network. Here, a "virtual callosotomy" is performed on the healthy control brains, creating control connectomes without callosal connections. Using the virtual callostomy approach, we can assess the changes in the connectome of the normal brain due to the absence of interhemispheric callosal connections, and use these findings to generate specific hypotheses for the AgCC connectome. Similarly, a "virtual Probstotomy" is performed on the AgCC cohort to demonstrate the contribution of the Probst bundles to the AgCC connectome.

Using a multi-scale connectomics analysis, we test three central hypotheses about the altered connectivity of AgCC subjects, garnered from the comparison of the controls to the virtual callosotomy case. First, we hypothesize that the AgCC brain has reduced long-range or global connectivity compared to the controls but increased short-range or local connectivity. Second, we expect to find that the AgCC connectome is less variable compared to the controls. Third, we postulate that the modular organization of the AgCC brain will not be altered due to the absence of the callosal fibers. While we do not assume that the virtual callosotomy will exactly replicate the AgCC brain, we do expect any deviations to provide insight into the structural alterations of AgCC beyond the lack of callosal connections.

Methods

Subjects

Written informed consent was obtained from all participants and/or their legal guardians under a study protocol approved by the institutional review board at our medical center. Seven subjects with AgCC (4 male, 3 female; mean age 24.3±14.2, 5 right-handed) and 11 healthy volunteers (6 male, 5 female; mean age 24.9±9.1, 11 right-handed) were included in

NIH-PA Author Manuscript

NIH-PA Author Manuscript

NIH-PA Author Manuscript

this study. Full-scale IQ was obtained from the AgCC cohort (mean FS-IQ 102±14) and control subjects (mean FS-IQ 109 ±17). A two-sample Student's t-test revealed that there was no significant group difference in age (p=0.92) or IQ (p=0.28) and a two-sample Fisher's exact test showed that there was no significant group difference in handedness (p=0.14) or gender (p=0.99).

Image Acquisition

All MR imaging was performed on a 3T EXCITE MR scanner (GE Healthcare, Waukesha, WI, USA) using an 8-channel head phased-array radio-frequency head coil. High-resolution structural MR imaging of the brain was performed with an axial 3D inversion recovery fast spoiled gradient-recalled-echo T1-weighted sequence (TE =1.5 ms, TR = 6.3 ms, TI=400 ms, flip angle of 15°) with a 230 mm FOV, and one hundred fifty-six 1.0 mm contiguous partitions at a 256×256 matrix. Structural MR images of all subjects were interpreted by an attending neuroradiologist certified by the American Board of Radiology.

Whole-brain diffusion was performed with a multislice 2D single-shot spin-echo echo-planar sequence with 55 diffusion-encoding directions, the array spatial sensitivity encoding technique for parallel imaging with a reduction factor of 2, a diffusion-weighting strength of b = 1000 s/mm^2; TR/TE=14,000/63 ms; NEX=1; interleaved 1.8-mm axial sections with no gap; in-plane resolution of 1.8 × 1.8 mm with a 128×128 matrix; and a field of view of 230 mm. An additional image set was acquired with minimal diffusion weighting (b =10 s/mm^2). The total acquisition time for diffusion imaging was 13 minutes.

Data Pre-processing

After non-brain tissue was removed using the Brain Extraction Tool (BET; http://www.fmrib.ox.ac.uk/analysis/research/bet/) with a fractional intensity threshold of 0.3 (Smith 2002), the diffusion-weighted images were corrected for motion and eddy currents using FMRIB's Linear Image Registration Tool (FLIRT; www.fmrib.ox.ac.uk/fsl/flirt) with 12-parameter linear image registration (Jenkinson et al., 2002). All diffusion-weighted images were registered to the reference b = 10 s/mm^2 image. From the transformation of every diffusion-weighted volume to the b = 10 s/mm^2 image, a scalar was derived, which reflects the amount each volume must be corrected. The mean of the parameter across volumes for each subject was used as the motion correction parameter in the *Data Quality Assurance* analysis. This procedure is described in a FMRIB technical report (Jenkinson, 1999). The fractional anisotropy (FA) image was calculated using FSL's DTIFIT.

Cortical Parcellation

The T1-weighted MR images were automatically segmented using FreeSurfer 5.1.0 (Fischl et al., 2004) with the default settings of recon-all, resulting in 68 cortical regions, 34 per hemisphere, and 14 subcortical regions, 7 per hemisphere. These 82 regions represent the nodes of the network and were used as the seeds for the fiber tractography described in the following section. A neuroradiologist confirmed the accuracy of the segmentation of the AgCC and control brains.

NIH-PA Author Manuscript

NIH-PA Author Manuscript

NIH-PA Author Manuscript

Fiber Tractography

Probabilistic tractography was performed with probtrackx2 (Behrens et al, 2007), with 2000 streamlines initiated from each seed voxel using the default options. Probtrackx2 allows for the inclusion of a termination mask, which halts tracking when a streamline comes into contact with a voxel in the mask. A termination mask was created by thresholding the FA image at FA<0.15, which prevents errant tracking across the interhemispheric fissure and between neighboring gyri through the sulcal space. In addition, a plane through the midline of the brainstem was manually drawn and was added to the termination mask in order to prevent descending streamlines from crossing the brainstem to ascend on the contralateral side.

The 68 cortical regions were transformed to the gray/white matter boundary (GWB) using FreeSurfer. Using FLIRT, the affine transform from diffusion to structural space was calculated by registering the FA volume to the T1 volume, then this transformation was inverted in order to register the FreeSurfer parcellation to the FA map. Each of the GWB volumes and the subcortical volumes was registered to the diffusion space to be used as seeds for the tractography. In order to regularize the seeding across cortical and subcortical areas, the seed regions in diffusion space were masked according to 0.15<FA<0.35. Each of the 82 seed regions was used in a separate tracking run and the results were compiled in a manner described in the next section, entitled “Connectome Reconstruction”.

To perform a virtual callosotomy for each of the control subjects, we repeated the above procedure with the addition of another exclusion mask. In probtrackx2, an exclusion mask can be utilized to exclude any streamlines that come into contact with the mask. A midline sagittal plane was manually drawn over the corpus callosum for each control subject. The addition of this exclusion criterion effectively removes any streamlines that pass through the corpus callosum. The networks derived from this procedure are referred to as “virtual callosotomy” connectomes.

Echoing the virtual callosotomy maneuver on the controls, a virtual Probstotomy was performed by placing an exclusion mask across a coronal cross-section of the left and right Probst bundles in the seven AgCC subjects. The Probst bundle exclusion masks were manually drawn on a coronal slice of the FA image approximately in the middle of the tract, for each subject, taking care not to include the cingulum bundle. We repeated the tractography with this exclusion mask and reconstructed the individual connectomes as described in the next section. The placement of all exclusion masks was checked by an attending neuroradiologist certified by the American Board of Radiology and with many years of experience with diffusion tractography to confirm that each mask only contains the tract of interest and that it contains the entire cross-sectional area of the tract on the two-dimensional image used to define the mask. Examples of the exclusion masks for virtual callosotomy and virtual Probstotomy are shown in Supplementary Figure S1.

Connectome Reconstruction

The technique used to construct the individual and consensus connectomes was modeled on standard processing pipelines found in the literature, including the use of FreeSurfer to

NIH-PA Author Manuscript

NIH-PA Author Manuscript

NIH-PA Author Manuscript

define the nodes of the network (Hagmann et al., 2007; Li et al., 2012a; Li et al., 2012b; van den Heuvel and Sporns, 2011). The pipeline, depicted in Figure 1, is most similar to the M2 method reported by Li et al., (2012a). The network analysis tools, described in the next section, are also conventional methodologies.

Each of the seed's tracking results were masked by each of the other 81 regions, referred to as targets, and summed across voxels to obtain a connection strength between each seed and target pair, effectively taking the total number of streamlines connecting two regions as the connection strength. This connection strength was then divided by the sum of voxels in the seed and target region to account for differences in volume between the various cortical and subcortical regions. Since tractography cannot determine directionality due to the antipodal symmetry of diffusion imaging, the normalized connection strength between each seed and target pair in both directions was summed and the connection strength of a seed with itself was set to zero. The resulting connection matrix is a symmetric matrix and yields two undirected connectomes for each control, one before and one after virtual callosotomy, and for each AgCC subject, one before and one after virtual Probstotomy. In network analysis terms, the 82 brain regions are the "nodes" and the connection strengths are the "edges" that connect the nodes. The edges can be weighted by the connection strengths, or can be binarized using a threshold on the connection strengths, as discussed below.

To create a consensus connectome for each of the three groups, the networks were first thresholded at a liberal level to remove the weakest connections, those less than approximately 0.5% of the maximum strength, which corresponds to a connection strength threshold of 6.5. Then, only those connections that exist in at least 75% of subjects in the group were retained and the connection strengths were averaged across subjects. The consensus network is binarized using the same threshold applied to the individuals, yielding three unweighted consensus connectomes: for the controls, virtual callosotomy controls, and AgCC subjects. The threshold was tuned in order to obtain a mean degree of approximately 12 for the control consensus connectome, based on published results (van den Heuvel and Sporns, 2011). For analyses of the individual connectomes, the same threshold of 6.5 was applied to binarize the networks. The effect of the threshold used on both the individual and consensus connectomes was explored by plotting mean degree, mean characteristic path length, and mean clustering coefficient at a wide range of thresholds, from approximately 0.05% to 12.5% of the maximum strength (Supplementary Materials).

Network Analysis: Summary Metrics

To test our hypothesis that the AgCC brain has decreased long-range connectivity, we calculate mean degree, characteristic path length, mean normalized betweenness, global efficiency, and cost. To test our hypothesis that the AgCC brain has increased short-range connectivity, we employ mean local efficiency and mean clustering coefficient.

The degree of a node is the number of connections that node makes with other nodes in the network. Characteristic path length is the average of the shortest paths between all pairs of nodes in the network, which is related to how quickly information can be transmitted through a network. Normalized betweenness is the number of shortest paths that pass through each node and is normalized to one if all the shortest paths, between all pairs of

NIH-PA Author Manuscript

NIH-PA Author Manuscript

NIH-PA Author Manuscript

nodes, pass through a particular node in the network. Normalized betweenness provides a measure of how centralized are the shortest paths. Global efficiency effectively takes the mean inverse path length between all pairs of nodes. This measure is similar to characteristic path length, but the inversion process reduces the disproportionate effect of long or infinite path lengths occurring in very sparse or disconnected networks.

Local efficiency is the mean inverse of the shortest path length between all nodes that pass through the connected neighbors of a node. Local efficiency provides a measure of the efficiency of the local environment of a node. Clustering coefficient takes the ratio of closed triangles between triplets of nodes and the number of connected triplets. Intuitively, a high clustering coefficient means that, if a node is connected to two other nodes, then those two nodes also likely to be connected to each other. This pattern of connectivity is assumed to be a hallmark of local integration of information. The reader is referred to Rubinov and Sporns (2010) and Bullmore and Bassett (2011) for a more comprehensive discussion of these network metrics, their significance and mathematic formulation. Only the cost metric is not defined in Rubinov and Sporns (2010). We calculate cost by dividing the number of suprathreshold edges by the total number of possible edges in the network.

The metrics were computed for the unweighted individual and consensus connectomes for comparison to previously published results on the normal human connectome. For the individual networks, the mean and standard deviation are calculated across the individuals in the group for each network metric. We also apply the weighted analogs of the network metrics that take the connection strengths into account to confirm our findings with the unweighted metrics for the AgCC subjects: mean strength (weighted analog to degree), weighted characteristic path length, mean weighted normalized betweenness, weighted global efficiency, mean weighted local efficiency, and mean weighted clustering coefficient. These weighted metrics are applied to the individual connectomes of the controls and AgCC subjects without any thresholding.

Network Analysis: Node Degree Distribution and Edge Consistency

To test if the spatial distribution of node degree was more variable between groups, we transform the degrees of the 82 nodes in each connectome into a vector and use the correlation coefficient in a pair-wise fashion between all the individuals in each group. In addition to assessing the variability of node degree, the correlation coefficient of the connection strengths was used as a measure of consistency for the networks as a whole. To quantify consistency between networks, we are interested in a network similarity metric. This is closely related to the problem of defining a "kernel" between graphs, a problem that has recently received much attention in the machine learning literature (Vishwanathan et al., 2010). One popular solution originally developed for comparing the structure of large molecules is based on comparing walks in the networks (Kashima et al., 2003), which is particularly well-suited for labeled graphs such as the human connectome. The simplest form of this is to compare all of the one-step walks in the graphs, which is equivalent to taking the correlation coefficient of the edge weights (i.e. connection strengths). Essentially, we are performing the simplest imaginable kernel (or similarity metric) between two graphs. This metric has therefore been used in two prior studies of the structural connectome to

NIH-PA Author Manuscript

NIH-PA Author Manuscript

NIH-PA Author Manuscript

measure network similarity (Hagmann et al., 2008; Bassett et al., 2011). In our investigation, the mean correlation coefficient was calculated between the consensus network and each individual network. The mean correlation coefficient was also calculated in a pair-wise fashion between the individual networks.

Network Analysis: Modularity

The weighted consensus and individual connectomes were decomposed into modules using a community detection algorithm proposed in Blondel et al. (2008). The problem of community detection requires the partitioning of a network into modules where nodes within the module are densely connected, while nodes belonging to different modules are only sparsely connected. Modularity and mean participation coefficient, both defined in Rubinov and Sporns (2010), were calculated for each partitioning of the consensus and individual connectomes. The mean and standard deviation were calculated for the individual connectomes. Modularity quantifies how well the module assignments are able to maximize intramodular connections, while minimizing intermodular connections. The participation coefficient quantifies the diversity of intermodular connections that a node makes. In addition, the stability of the modular assignment was quantified using the Hubert rand index (Hubert and Baker, 1977). Mean Hubert rand index was computed in two ways for each of the three groups: 1) between the modular assignment for each of the individual connectomes and the assignment for the consensus connectome, and 2) pair-wise between the modular assignments for the individual connectomes. The modular assignments are nondeterministic because of dependence on initial conditions for the optimization; therefore, for the consensus connectomes, the modular assignment that appeared most often across multiple runs with 100 random initial conditions was selected. For the individual connectomes, the module assignment algorithm was repeated 100 times with random initial conditions and the mean and other descriptive statistics of the network metrics were computed over these multiple iterations. The code used to compute the network measures and the modules is part of the open-source Brain Connectivity Toolbox (https://sites.google.com/site/bctnet), described in Rubinov and Sporns (2010).

Network Analysis: Statistical Inference Testing

To assess the statistical significance of between-group comparisons of the network metrics and the measures of connectome variability described above, a non-parametric permutation testing procedure was used. For each metric, the data labels were randomly reassigned between the two groups and t-values were computed for each relabeling, for a total of 5000 permutations. P-values were calculated based on the distribution of t-values obtained from the permutations and a threshold of $p<0.05$ was used to determine significance. The strength of connections in the anterior-posterior edges of modules corresponding to the “structural core” of the cerebral cortex (Hagmann et al., 2008) was tested for statistical significance between the control and AgCC groups using the same permutation test described above. We take a data-driven approach to the definition of the structural core, in that the structural core was taken to be the module comprised of the medial cortical regions in each cerebral hemisphere. The p-values obtained were adjusted for multiple comparisons with a false-discovery rate (FDR) correction.

NIH-PA Author Manuscript

NIH-PA Author Manuscript

NIH-PA Author Manuscript

Network Analysis: Virtual Probstotomy

After obtaining connectomes for AgCC with the Probst bundle connections removed bilaterally, the percent difference of each connection strength between all pairs of nodes was calculated, generating a percent difference matrix for each subject. The mean and standard deviation for each subject was computed and the percent difference matrices were binarized based on a threshold of mean plus one standard deviation, calculated for each subject. The binarized percent difference matrices were added in order to obtain a consensus percent difference matrix (with a minimum of 0 and a maximum value of 7) that reflects the connections most commonly affected by the absence of the Probst bundles.

Data Quality Assurance

The following quality control metrics were calculated a) the mean motion correction parameter, b) white and gray matter volumes (obtained from FreeSurfer), and c) IQ. These variables were correlated with mean degree for the individual connectomes and p-values were obtained. This analysis was performed to determine if the differences in the network metrics could be explained by an imaging artifact such as motion, or factors related to demographics such as IQ, or to anatomical characteristics such as gray and white matter volumes. Furthermore, we also correlated a) mean FA for the entire brain, b) mean FA for the seed regions and c) mean of the seed volumes with mean degree of the individual connectomes to ensure that inter-subject variation in these measures did not inject potential sources of bias into the analyses. A Kolmogorov-Smirnov test between the healthy controls and AgCC was computed to determine if there were any statistically significant group differences.

Results

Brain Anatomy

Two color fractional anisotropy maps are displayed in Figure 2. On the top row, the brain of a healthy control is shown; in the midline sagittal image, both the corpus callosum and anterior commissure are seen in red due to the left-right orientation of their axonal fibers. In the bottom row, the brain of a subject with AgCC, the complete absence of a corpus callosum is observed, while the anterior commissure is intact and is relatively large in cross-sectional area compared to the control. In the coronal image for the AgCC subject, the Probst bundles running anterior-posterior are seen in green.

All high-resolution 3D T1-weighted images of the AgCC subjects and controls were reviewed by a board-certified neuroradiologist. The control brains were free of structural anomalies and the acallosal brains were free of any additional structural anomalies commonly found in association with AgCC, such as heterotopias, abnormal sulcation, or hindbrain anomalies (Hetts et al., 2006). All 7 AgCC participants had complete absence of the corpus callosum, distinguishing their condition from patients with so-called “partial agenesis of the corpus callosum”, also known as “hypogenesis of the corpus callosum” (Hetts et al., 2006; Wahl et al., 2009). Hence, the seven AgCC individuals in this study may be considered to have “isolated complete AgCC”, i.e. complete absence of the corpus callosum without other associated abnormalities visible on conventional MRI.

NIH-PA Author Manuscript

NIH-PA Author Manuscript

NIH-PA Author Manuscript

Data Quality Assurance

There were no significant correlations between mean degree and any of the nuisance variables considered: mean motion correction, mean FA for the entire brain, mean FA for the seed regions, mean of the seed volumes, white and gray matter volumes, and IQ. There were also no significant group differences in these variables between the AgCC and control cohorts ($p>0.05$). Notably, this indicates that subject motion during the scan was not worse for AgCC than for the normal volunteers.

Consensus Connectomes

The consensus connectomes for the three groups are shown in Figure 3. Each circle represents a seed region or “node” (plotted at the centroid of each FreeSurfer parcel) and a line connecting two seed regions, or “edge”, represents a structural connection between the regions. The color and size of each node indicates its degree, where six equally-spaced bins have been selected, as illustrated in the legend, and the weight of each edge is scaled by the strength of its connectivity. The nodes have been labeled according to the abbreviations listed above in the *Abbreviations section* and the connectomes are plotted in the neurological convention, i.e. the left hemisphere is shown on the left side of the image and vice versa.

In Figure 4, the degree of each node in the three consensus connectomes has been plotted in descending order. The nodes in the brain with the highest degree are often referred to as “hubs”. Here, any node with degree greater than the mean degree plus one standard deviation is designated as a hub, following Li et al. (2012a) as well as van den Heuvel and Sporns (2011). For the control consensus connectome (Figure 4a), these regions include bilateral putamen, bilateral thalamus, bilateral precuneus, left superior frontal, right insula, and left superior parietal, indicated by the red color. The homologous regions contralateral to the unilateral hubs also have high degree, but do not meet the criterion for being hubs. The plot for the virtual callosotomy controls and AgCC has been colored according to the hubs in the control consensus and the dotted line indicates the mean plus one standard deviation cutoff. Thus, any nodes colored red appearing to the right of the dotted line have been demoted from hub status and any white bars to the left of the dotted line are nodes that have been promoted. In the virtual callosotomy controls, four cortical nodes have been demoted (bilateral precuneus, right superior parietal, and left superior frontal), while the rest of the hubs are preserved. Conversely, the bilateral superior temporal regions are promoted to hub status in the virtual callosotomy controls. In the AgCC consensus, only the precuneus regions on both sides are demoted from hub status; however, their degrees are both much lower than seen in the virtual callostomy consensus. The nodes promoted to hub status in the AgCC consensus connectome are quite different than the virtual callosotomy case: specifically, the left insula, bilateral caudate, right superior frontal, and left superior parietal are elevated to hub status. Overall, these findings suggest that absence of the corpus callosum alone cannot explain the degree distribution of the consensus AgCC connectome.

Mean degree, characteristic path length, mean betweenness, global efficiency, cost, mean local efficiency, and mean clustering coefficient were calculated for the three consensus connectomes (Table 1). There is an apparent decrease in mean degree, global efficiency, and cost in both the virtual callosotomy controls and AgCC subjects relative to the controls.

NIH-PA Author Manuscript

NIH-PA Author Manuscript

NIH-PA Author Manuscript

There is an apparent increase in characteristic path length, mean betweenness, mean local efficiency, and mean clustering coefficient in the virtual callosotomy controls and AgCC subjects compared to the controls. However, these apparent group differences in the summary network metrics of the consensus connectomes cannot be supported statistically, since there is only one instance of the consensus connectome for each group. This motivates further analysis of individual connectomes.

Individual Connectomes

Examples of individual connectomes for three controls and three AgCC subjects are shown in Figure 5. The controls in the left column illustrate the similarity between the structural connectomes of individual normal volunteers. Qualitatively, the spatial distribution of high and low degree nodes does not change dramatically between the individuals. In contradistinction, the AgCC connectomes visually demonstrate more variability between individuals in the location of the high and low degree nodes. In order to quantify these qualitative observations, we examined the within-group node degree variability as described in the Methods section. We found that the spatial distribution of node degrees was indeed significantly more variable in the AgCC group as demonstrated by a lower mean correlation coefficient ($r=0.78\pm0.05$) compared to the controls ($r=0.81\pm0.03$) at $p<0.05$.

To further quantify these qualitative differences between groups, the connection strength correlation coefficient was calculated between each individual connectome and its group consensus connectome as well as between every pair of individual connectomes in each group. The results of this analysis are presented in Table 2, where it is evident that the consensus connectomes of the three groups represent the individuals in their group to approximately the same extent, with no statistically significant differences. However, the inter-individual variability of the AgCC connectome is greater than that of the control connectome, as shown by a significantly lower consistency between individual networks. This is opposite to the virtual callosotomy connectomes, which are slightly more similar to one another than is the case for the individual control connectomes. Hence, the correlation coefficients of the degree spatial distributions and the connection strengths both support the qualitative impression from Figure 5 that the AgCC connectomes are more variable than the control connectomes.

In Figure 6, the degree of each node, averaged across subjects, is plotted in descending order for the individual connectomes for the three groups. The standard deviation of the degree across individuals is plotted as an error bar for each node. Hubs are defined as those nodes with degree greater than the mean degree (across all nodes) plus one standard deviation. This is the same definition used with the consensus connectomes. The hubs for the controls are bilateral putamen, bilateral thalamus, bilateral precuneus, bilateral superior parietal, right insula, and left superior frontal (Figure 6a). The virtual callosotomy results demonstrate that bilateral precuneus and left superior frontal are demoted from hub status when the callosal connections are excluded, whereas bilateral superior temporal, left insula, and left pallidum are promoted to hub status (Figure 6b). The AgCC individuals also show demotion of bilateral precuneus and left superior frontal, as well as promotion of the left insula and left

NIH-PA Author Manuscript

NIH-PA Author Manuscript

NIH-PA Author Manuscript

pallidum; however, the other three new hub nodes (the bilateral caudate and right pallidum) are different from the virtual callosotomy case (Figure 6c).

Descriptive statistics of mean degree, characteristic path length, mean normalized betweenness, mean clustering coefficient, global efficiency, and cost calculated for each individual connectome in the three groups are presented in Table 3. All of the metrics were found to be significantly different ($p<0.05$) between the control and virtual callosotomy groups. Characteristic path length, mean normalized betweenness, global efficiency, mean local efficiency, and mean clustering coefficient were also found to be significantly different between the control and the AgCC groups, and in the same direction (i.e. higher or lower) as the differences between the control and virtual callosotomy groups. However, differences in mean degree and cost were not statistically significant between control and AgCC groups, even though the trends in these metrics were also in the same direction as that between control and virtual callosotomy groups.

In order to test post hoc for differences in within-hemisphere connectivity between controls and AgCC, we computed the summary graph metrics for only the intrahemispheric connections of the right and left cerebral hemispheres. Examining the average unweighted network metric values of the right and left hemispheres, the mean degree, mean clustering coefficient, global efficiency, and mean local efficiency all trend higher in AgCC compared to controls, whereas the characteristic path length and mean normalized betweenness both trend lower in AgCC than controls. However, none of these trends reach statistical significance, with clustering coefficient and mean local efficiency being the metrics with the strongest group differences at $p<0.09$.

Modularity Analysis

A community detection algorithm was applied to the consensus and individual connectomes in the three groups. The module assignments for the consensus connectomes are shown in Figure 8. Seven modules are present in the control and virtual callosotomy consensus connectomes, (Figure 7a and 7b, respectively). The assignments for these two groups are identical. There are two modules, Module 1 and Module 5, which together make up the “structural core” of the network (Hagmann et al., 2008). Modules 3 and 6 largely consist of frontal nodes, while Modules 2 and 7 are more posterior. On the left, a subcortical module breaks off into Module 4. The mean modularity for the control and virtual callosotomy groups is 0.58 and 0.60, respectively, and mean participation coefficient is 0.32 and 0.25, respectively. There are 6 modules assigned to the AgCC consensus connectome (Figure 7c) and the assignment is quite different from that found for the control and virtual callosotomy consensus connectomes. Most notably, the structural core in each hemisphere is not separate from the other modules, indicating a breakdown of the preferential anterior-posterior connectivity in this sub-network. There is perfect bilateral symmetry of the modules in the community assignments for the AgCC consensus connectome, which is not observed in the control or virtual callosotomy cohorts. The mean modularity for the AgCC consensus connectome is 0.59 and mean participation coefficient is 0.26.

Due to space constraints, the modularity assignments for each individual connectome are not shown. In lieu of these results, the mean and standard deviation of modularity-related

NIH-PA Author Manuscript

NIH-PA Author Manuscript

NIH-PA Author Manuscript

metrics are provided in Table 4. The mean modularity of the individual connectomes is significantly greater in the virtual callosotomy group compared to the controls, but not in the AgCC group compared to the controls. Relative to controls, the mean participation coefficient is significantly decreased in both the virtual callosotomy group and the AgCC group. The Hubert rand index computed between the individual module assignments and the consensus module assignment is significantly different between the controls and AgCC groups, and the Hubert rand index computed between the module assignments for all pairs of individuals is significantly decreased in both the virtual callosotomy and the AgCC groups as compared to the controls.

The Structural Core of the Cerebral Cortex in AgCC

The weakening of the structural core in AgCC leads to the hypothesis that the connection strengths among the nodes that normally form the structural core of the cerebral cortex are abnormally decreased in AgCC. The structural core nodes are taken to be those that belong to Modules 1 and 5 of the control consensus connectome: caudal anterior cingulate, posterior cingulate, paracentral lobule, isthmus of the cingulate, and precuneus in both hemispheres. The strength of these twenty intrahemispheric connections was tested post-hoc for group differences between AgCC and controls, correcting for multiple comparisons with FDR. Interhemispheric connections between these regions do not exist in the acallosal brain and therefore could not be tested. The results are shown in Figure 8. Six of the twenty connections are found to be significantly reduced in strength in AgCC ($p<0.05$); in fact, these six edges represented all of the possible connections among regions of the cingulate cortex (CAC, PCC, and ISC) within each hemisphere.

In addition to testing for statistical differences in connection strengths within the structural core of the controls and AgCC, we also assessed whether the structural core was present in its entirety in each of the individual connectomes for the controls and AgCC. Again, we are defining the structural core as containing the five bilateral, medial nodes found in the modular partition of the control consensus connectome in this study. We found that 9 of the 11 controls have a complete structural core. The 2 control subjects without a complete structural core have an intact structural core module in the left hemisphere, but the module that would be the right half of the structural core includes lateral nodes in one case and is split anterior-posterior in the other case. On the other hand, none of the individual AgCC connectomes contain a complete structural core. In each AgCC individual, the structural core is split into separate anterior and posterior modules. In most cases, these anterior and posterior modules also include more lateral nodes, as also seen in the module assignments for the consensus AgCC connectome (Figure 7c).

Virtual Probstotomy in AgCC

In Figure 9, the results of the virtual Probstotomy on the AgCC subjects are presented. Figure 9a shows the consensus percent difference matrix for all edges in the connectome. The maximum consensus observed was six out of the seven subjects and only connections that were affected in at least three of the seven subjects are displayed. In Figure 9b, the edges of the connectome that were altered by the virtual Probstotomy in three or more of the seven AgCC subjects are displayed. Both panels of Figure 9 demonstrate that the Probst

NIH-PA Author Manuscript

NIH-PA Author Manuscript

NIH-PA Author Manuscript

bundles contain a mixture of subcortical to subcortical, subcortical to cortical, and corticocortical connections. Not surprisingly, the greatest connectivity is within paramedian regions of each cerebral hemisphere, including subcortical structures, with no connections seen to lateral cortical regions. Overall, these results demonstrate that the connectivity of the Probst bundles exhibit moderate to high consistency across subjects and a high degree of hemispheric symmetry.

Discussion

The AgCC Connectome: More than Just the Absence of Callosal Fibers

Using a multi-scale connectomic analysis, we tested three main hypotheses concerning the altered connectivity of the acallosal brain using virtual callosotomy to generate the hypotheses and data from AgCC subjects to support or reject the hypotheses. The first hypothesis is that global connectivity would be reduced and local connectivity would be increased in AgCC versus controls, as demonstrated by the virtual callosotomy case. Table 3 shows that the global connectivity part of the hypothesis was confirmed by the significant decrease in global efficiency as well as the increase in both characteristic path length and mean normalized betweenness of AgCC versus controls. The local connectivity part of the hypothesis was also confirmed by the significant increase in mean local efficiency and increase in mean clustering coefficient of AgCC versus controls. These were the same changes of the summary graph metrics seen in virtual callosotomy versus controls. Notably, the mean degree did not differ significantly between control and AgCC groups (Table 3). This means that comparisons of graph metrics between the two groups are not biased by group differences in the density of network connections (Anderson et al., 1999).

The second hypothesis is that the AgCC connectome would be less variable than the control connectome, as found in the virtual callosotomy case where the inter-individual network consistency was significantly greater than that of controls (Table 2). This prediction makes intuitive sense, since removal of callosal connections reduces the number of links that might differ across networks. However, this hypothesis was rejected by the same analysis of AgCC connectomes, which actually exhibited much lower consistency than that of controls (Table 2). The increased variability of the AgCC connectome was also reinforced by the significantly greater variation in the spatial distribution of node degrees compared to controls.

The third hypothesis is that the modular organization of the AgCC brain does not differ from that of controls, as suggested by virtual callosotomy (Figure 7a,b). This hypothesis was also rejected, as is apparent from the very different modular assignments of the AgCC consensus connectome (Figure 7c). Moreover, Table 4 shows that the similarity of modular assignments between the individual AgCC connectomes and the consensus AgCC connectome is significantly less than that between the individual control connectomes and the consensus control connectome, a difference not anticipated by the virtual callosotomy case. Although virtual callosotomy predicts a slight but significant decrease in consistency of inter-individual modular assignments compared to controls, the actual observed difference is much larger for the AgCC group (Table 4). This is also consistent with the topology of white matter connectivity in AgCC being more variable across subjects than is

NIH-PA Author Manuscript

NIH-PA Author Manuscript

NIH-PA Author Manuscript

the case for controls. Finally, using modularity analysis to identify the “structural core” of the cerebral cortex, the connections within this bilateral sub-network are found to be weaker in subjects with AgCC than in controls, especially in the cingulate bundles bilaterally.

Together, these observations demonstrate that structural connectivity in AgCC, a classic axonal pathfinding disorder, is much more complex than can be explained by the simple absence of callosal connectivity. Although the virtual callostomy model correctly predicted the direction of changes in summary graph metrics to be found in the acallosal brain, the estimates for more sophisticated properties of the network such as its topological variability and modular structure were found to be incorrect. The implications of this are explored in more detail below.

MR Connectomics of a Prototypical Axon Guidance Disorder

To our knowledge, this study is the first to apply MR connectomics to a congenital human brain malformation. One important feature of the structural connectome framework is the ability to study the effect on white matter connectivity of virtual lesions. This approach has been employed to generate white matter importance maps in a prior study of traumatic brain injury by systematically deleting all edges of the connectome that pass through a certain node, i.e., all fiber tracts connecting a specific brain region, and then recalculating global network metrics to assess the “importance” of each node (Kuceyeski et al, 2011). The virtual lesion technique is particularly well suited for investigating axonal pathfinding disorders, since it can be used to determine the changes in connectivity due to absent tracts as well as ectopic tracts and can be utilized to generate hypotheses about patient populations with stereotyped lesions.

The virtual callostomy maneuver reveals how removal of all callosal connections affects the normal human connectome. We show that, although many of the significant differences in summary graph metrics between the controls and AgCC are reproduced by the virtual callostomy case, there are key differences in their results for network consistency and modular architecture. This is in agreement with hypotheses about probable molecular defects in axonal guidance underlying the disorder, which might be expected to affect more than just the corpus callosum. Another interpretation of these results would be that there is compensatory rewiring in AgCC to circumvent the absence of direct callosal connections between the two cerebral hemispheres. These two explanations are not mutually exclusive and their effects would be difficult to disambiguate. This remains an area for future investigation.

The power of connectomics to elucidate the connectivity of ectopic tracts is demonstrated by the virtual Probstotomy that we applied to the AgCC connectome. We observe that the fibers of the Probst bundles connect certain brain regions with some consistency and these connections can be corticocortical as well as subcortical-subcortical and subcortical-cortical (Figure 9). The subcortical connectivity of the Probst bundles is supported by prior investigation in mouse models of AgCC (Ren et al., 2008), but not fully anticipated by prior diffusion tractography studies in humans. Hence, in AgCC, the interhemispheric corticocortical connectivity of the corpus callosum is instead rewired into intrahemispheric connections, some of which are subcortical. These changes to inter- and intrahemispheric

NIH-PA Author Manuscript

NIH-PA Author Manuscript

NIH-PA Author Manuscript

connectivity are also evident in the degree distributions (Figures 4 and 6). Virtual callosotomy of the normal human connectome causes a drastic reduction in the degree of paramedian cortical hubs, such as superior frontal and superior parietal cortex, while the AgCC connectome preserves these regions as hubs or only mildly reduces their degree. The preserved connectivity of these regions must be due to increased connectivity with intrahemispheric brain areas. In addition, the subcortical regions tend to be more connected in the AgCC connectome than in the control connectome, either with or without virtual callostomy. It is probable that a combination of increased connectivity through the anterior commissure and the Probst bundles contributes to these discrepancies between the AgCC and virtual callosotomy connectomes.

While some brain areas are consistently connected through the Probst bundle in almost all the examined AgCC subjects, there are also a number of connections that are found in only three or four of the seven AgCC individuals. The limited findings from prior research include a diffusion tensor imaging (DTI) and high angular resolution diffusion imaging (HARDI) tractography study of subjects with partial AgCC that showed that the topography of the callosal connections in these individuals is highly variable and that there are both homotopic and heterotopic connections which do not necessarily correspond to the position or size of the corpus callosum fragment (Wahl et al., 2009). Another DTI tractography study (Tovar-Moll et al., 2007) reported similar results, showing that the partial AgCC brain has a combination of normal and aberrant callosal connections, and the correspondence between the location of the partial corpus callosum does not perfectly correlate with the cortical regions established in the healthy control brain (Hofer and Frahm, 2006). These findings, when combined, provide solid evidence that there is substantial inter-individual variability and aberrant connectivity both in the Probst bundles of AgCC subjects and in the callosal fibers of partial AgCC.

Summary Network Metrics

The summary network metrics from the control consensus connectome of our study (Table 1) are very similar to those reported in a recent study of the normal human connectome (van den Heuvel and Sporns, 2011), supporting the validity of our methods, although one of these metrics, the mean degree, was deliberately matched to the prior study in order to set the connectivity threshold for reconstruction of the connectomes. This general agreement is also consistent with prior results showing high test-retest reliability of graph metrics, even from imaging data acquired with different diffusion gradient acquisition schemes (Vaessen et al., 2010), as well as moderate to high reliability of graph metrics across different methods for reconstructing connectomes from diffusion-weighted imaging data (Li et al., 2012a).

For the consensus connectomes, the summary network metrics for the virtual callosotomy and AgCC groups are similar and can be conflated as the threshold varies (Figure S2). However, the same is not true for the individual connectomes (Figure S2 and Table 1 and Table 3). To understand why, it is useful to understand the advantages and disadvantages of consensus connectomes versus individual connectomes. The consensus connectomes have the advantage of being pooled across all the individuals in the group, which smooths out individual variation and allows for comparison of graph metrics with other studies that have

NIH-PA Author Manuscript

NIH-PA Author Manuscript

NIH-PA Author Manuscript

reported results for consensus connectomes. However, examination of individual connectomes is needed to understand individual variation within a group as well as to establish statistically significant differences in network metrics between groups. Measures of edge consistency among individual connectomes show that individual AgCC connectomes are significantly more variable than individual control connectomes (Table 2). This finding was not predicted by the comparison of the controls to the virtual callosotomy case. This may explain the discrepancies between the network metrics applied to the individual versus the consensus connectomes, since greater variability among the edges of the individual AgCC connectomes would result in fewer of the edges being retained in the consensus AgCC connectome.

The network metrics applied to the individual connectomes reveal that, while there is a decrease in global efficiency and increase in characteristic path length and mean normalized betweenness comparing the control group to the virtual callosotomy and AgCC groups, the mean local efficiency and mean clustering coefficient is instead increased in the virtual callosotomy group and AgCC groups (Table 3). This pattern of differences in graph theoretic metrics of the control subjects before and after virtual callostomy is to be expected from the loss of long-range interhemispheric callosal fibers, which often interconnect cortical hubs and form by far the major route of information transmission between the two cerebral hemispheres. Mean normalized betweenness and characteristic path length are related in that, as the characteristic path length increases, the number of nodes that the shortest paths go through should also increase. The increase in the measures of local connectivity (mean local efficiency and mean clustering coefficient) is less intuitive. Eliminating callosal connections has the effect of increasing the clustering coefficient because the callosal connections tend to be homotopic and do not participate in closed triangles. The increase in local efficiency is related to the increase in characteristic path length and mean normalized betweenness; more nodes have shortest paths that pass through them as the shortest paths get longer.

In the analysis of individual networks, although the AgCC connectome lacks callosal connections, the mean degree and cost are not significantly decreased compared to controls, unlike the virtual callostomy example (Table 3). This finding must be due to the presence of alternate pathways that are not present in the normal human connectome, such as the Probst bundles. These ectopic tracts maintain the cost and mean degree of the network at values similar to those of controls, but do not make up for the absence of interhemispheric callosal connections in sustaining the high global efficiency across both cerebral hemispheres of the control connectome.

The group differences between AgCC and controls observed with the unweighted graph metrics are largely confirmed with the weighted network metrics (Supplementary Table S1). However, weighted characteristic path length was not significantly increased in AgCC and mean weighted local efficiency was slightly decreased, instead of increased. One explanation for this discrepancy is that these weighted metrics involve the calculation of weighted path lengths. We have found weighted characteristic path length to be one of the least reliable network metrics as assessed with test-retest reproducibility data (unpublished results).

NIH-PA Author Manuscript

NIH-PA Author Manuscript

NIH-PA Author Manuscript

It is possible that enhanced intrahemispheric connectivity due to ectopic or compensatory fiber tracts might help account for the improved local efficiency in AgCC, as reflected in the higher mean clustering coefficient and mean local efficiency. This post hoc hypothesis was directly tested by computing the summary graph metrics for only the intrahemispheric connections of the right and left cerebral hemispheres. The pattern of differences in these metrics are what would be expected with enhanced intrahemispheric connectivity in AgCC; however, these trends did not reach statistical significance. Since it is likely that the small sample size of this study is underpowered to detect these subtler effects within subsets of the connectome, larger-scale investigations are needed to draw firm conclusions regarding whether intrahemispheric connectivity is enhanced in AgCC.

Degree Distribution and Hubs

Degree is a focus of the analysis of both the consensus networks and the individual networks, as it can identify the hubs of a network. Our identification of hub regions from individual normal connectomes based on node degree (Figure 6a) shows good agreement with Li et al. (2012a), with the majority of regions deemed to be hubs in Figure 6a also appearing as hubs in Li et al. (2012a) and vice versa. This correspondence with prior literature on the normal human connectome again provides external validation for our results. Many of the cortical hubs in the control connectome, in both the consensus and individual analyses, were demoted from hub status when the corpus callosum was virtually cut. There were also new hubs created from the exclusion of the corpus callosum. The consensus and individual analyses of AgCC reveal the demotion of cortical hubs and the promotion to hub status of several different nodes, including several subcortical areas. This comparison again shows that, in AgCC, the network topology is fundamentally reorganized in a way that cannot be entirely explained by the exclusion of callosal fibers from the normal human brain. The correlation of node degree among the individuals in each group reveals that the spatial distribution of node degree is more variable in the AgCC cohort as compared to the controls.

Modularity Analysis and the Structural Core of the Cerebral Cortex

Modular organization is conspicuously different for the AgCC consensus connectome compared to the control and virtual callosotomy consensus connectomes (Figure 7) and this finding was not predicted by the comparison of the controls to the virtual callosotomy controls. The most obvious difference is the weakened structural core of the cerebral cortex in AgCC. Therefore, even though the AgCC subjects have massive Probst bundles bilaterally, these tracts do not seem to meaningfully increase anterior-posterior corticocortical connection strengths among the medial cortical hubs that comprise the structural core. It was observed that AgCC has significantly reduced connectivity relative to controls between regions of the cingulate cortex that would normally form an important part of the structural core (Figure 8). This decrease in connectivity can help explain the difference in modular assignments of AgCC versus the normal connectomes. If there is not preferential wiring between paramedian cortical regions in AgCC, then these nodes do not become segregated into a distinct module by the community detection algorithm. This finding is concordant with evidence from DTI that the ventral cingulum in AgCC has reduced fractional anisotropy and reduced volume compared to control subjects (Nakata et

NIH-PA Author Manuscript

NIH-PA Author Manuscript

NIH-PA Author Manuscript

al., 2009), but also extends this prior observation to include the dorsal cingulum as well. Hence, data-driven modularity analysis of regional integration and segregation can discover abnormalities of connectivity across the whole-brain network in AgCC, at least one of which has been previously demonstrated by a more focused hypothesis-driven diffusion tractography study.

The significant decrease in participation coefficient found for both virtual callosotomy and for AgCC is not surprising, since the loss of long-range callosal connections would decrease the number of intermodular connections. The modularity of the virtual callosotomy connectomes was significantly greater than the controls, but the AgCC did not exhibit a significant change in modularity. The similarity in the modularity metric for the controls and AgCC indicates that it was not easier to partition one group over another, lending credibility to the differences we do detect in modular organization between the two groups.

The finding that the Hubert rand index is considerably lower for individual AgCC connectomes than for controls, both compared to the consensus connectome and compared to one another (Table 4), means that module assignments are less consistent among AgCC subjects than controls. Hence, modularity analysis provides more converging evidence that the AgCC connectome is more variable than that of the normal human brain. This increased variability of network modular organization cannot be explained solely by the lack of callosal connectivity, since the Hubert rand index of the individual virtual callosotomy connectomes versus that of their consensus connectome was not reduced compared to the same measure in controls.

Methodological Considerations and Study Limitations

We use a common approach to diffusion tractography for connectome reconstruction that was deliberately chosen to be conservative when comparing normal controls to acallosal brains. This technique relies on probabilistic streamline fiber tracking seeded from the GWB and permits tracking along intravoxel crossing fibers using HARDI data; as such, it hews closely to the M2 method of Li et al. (2012a). The effect of different tractography methods on connectome reconstruction was explored by Li et al. (2012a, 2012b). They found no significant advantage in accuracy of any particular technique over the others, using macaque tract-tracing data as the gold standard. However, they did find a fundamental difference between tractography seeded throughout the white matter (the M1 method) and tractography seeded from the GWB (the M2 method) in that the M1 method showed relatively stronger connectivity over long-range connections than did M2. This is because long-range tracts contain more seed regions in M1 and are therefore overemphasized, whereas connection probability decreases with distance in M2 and thus long-range connections are underemphasized. A variant of M2 that is normalized by tract volume to account for the decreasing connection probability with distance (the M3 method) did not significantly improve the accuracy of in vivo tractography in humans (Li et al. 2012a); nor did a newer global tractography approach (Li et al., 2012b). By adopting a fiber tracking method that is known to understate long-range connectivity such as through the corpus callosum, we are being conservative in our comparisons between the normal brain and those of AgCC subjects. Hence, it is possible that the observed differences between the normal connectome

NIH-PA Author Manuscript

NIH-PA Author Manuscript

NIH-PA Author Manuscript

and the AgCC connectome would have been greater if a less conservative tractography approach had been employed.

The various tractography methods used across different connectome studies make the edge weights (i.e. connection strengths) impossible to compare with the prior literature. As such, to have some comparability across studies, we apply graph metrics to unweighted graphs and analyze consensus connectomes along with individual connectomes and we confirm these findings with weighted metrics. We chose a common threshold across the groups, as opposed to thresholding each network to maintain a constant degree distribution or edge density, as is commonly done in the literature (van Wijk et al., 2010). Since the connection strengths are normalized by the seed and target volumes and there were no significant correlations between mean degree and white or gray matter volumes, it is defensible to apply the same threshold to the edge weights for the healthy controls and for AgCC. In the case of AgCC, using a common threshold reveals decreases and increases in connectivity that would not have been detected if the degree or density were held constant across groups. Along these lines, it is interesting that even though statistically significant group differences are detected in the individual connectomes for mean characteristic path length, mean normalized betweenness, mean clustering coefficient, and global efficiency, there was no statistically significant difference in mean degree of AgCC versus controls. The global network metrics we use here are not normalized by results from random networks; the small world coefficient is an example of a metric that requires such normalization. Since we use network metrics for group comparisons and not for drawing absolute inferences about network properties, such as small worldness, in isolation, there is not a strict necessity for metrics normalized by random networks.

FreeSurfer was used to segment the brain into 82 cortical and subcortical regions, representing the nodes of the network. Although no participants had visible cortical malformations, the gyral and sulcal anatomy of AgCC might still contain subtle divergence from the FreeSurfer atlas, which is based on the normal human brain. Hence, it is possible that differences in cortical parcellation might account for some of the connectomic differences observed between AgCC and controls. However, there is no evidence in the literature for major cortical reorganization in AgCC. Indeed, recent fMRI studies show a surprising degree of homology of functional connectivity networks between AgCC and normal brain (Khanna et al., 2012; Li et al., 2011; Lum et al, 2011; Tyszka et al., 2011). Furthermore, significant differences in global network metrics were observed in the AgCC cohort relative to controls that are not commensurate with the expected regional increases and decreases that would be caused by inconsistencies in cortical and subcortical parcellation. Given that there is not a significant correlation between mean degree and white or gray matter volumes for the AgCC group, the differences seen between the controls and AgCC and within the AgCC group are unlikely to be driven by the designation of cortical and subcortical boundaries.

Given that we exclude subjects with additional brain malformations besides AgCC and also those with partial agenesis of the corpus callosum, our sample size is limited to seven individuals with isolated complete AgCC. In addition to reducing statistical power, the small sample size of this pilot study also limits the ability to avoid bias in comparison with control

NIH-PA Author Manuscript

NIH-PA Author Manuscript

NIH-PA Author Manuscript

subjects. In this study, handedness is not matched between the experimental and control groups. Handedness is not always reported in the connectome literature and it is common practice in the connectome literature to combine networks from different individuals into a single consensus network. This is justified by the assumption that, at the coarse level of granularity of the cortical parcellation (100 nodes or less), there should be little biological variability among the connectomes of normal adult subjects regardless of demographic factors such as gender or handedness. Also, the effects of the gross alterations of white matter connectivity in AgCC are certain to be much larger than any effects of handedness. For these reasons, we did not feel that it was strictly necessary to match for handedness in this pilot study. This potential limitation can be addressed in future larger-scale connectomics studies that might focus on more subtle effects of neurodevelopmental disorders.

Future Directions

As discussed above, there are many levels of granularity at which the connectome can be explored and the definition of nodes is one way to modify the granularity. The FreeSurfer parcellation provides a way to segregate the brain into nodes, but the cortical and subcortical regions could be further segregated into many smaller regions up to the number of voxels in each region. As future work, we plan to investigate connectomes with thousands of nodes, which will provide a much richer and more detailed connectivity map. This will have particular advantages for AgCC, since the much smaller-sized regions of these more granular networks do not need to depend on anatomical boundaries defined on the normal brain. Another avenue of further investigation is the relationship between the functional and structural connectomes in AgCC.

Individuals with AgCC often suffer from impairments in higher-order cognition and social skills. These deficits overlap with the diagnostic criteria for autistic spectrum disorders (Paul et al., 2007). The connectome can provide global measures of brain organization that could be correlated with behavioral or cognitive outcome variables, as discussed above. The sample size of patients in this exploratory study of the AgCC connectome is too small to permit neurocognitive correlation. This will be a focus of future larger-scale investigations.

The pathophysiology of axonal guidance disorders and, more generally, of neurodevelopmental diseases is not thought to be limited to one or a few isolated brain regions. Instead, neural circuits diffusely throughout the cortex have been implicated and these illnesses are now considered to be connectopathies (Seung 2012). A leading hypothesis for autism postulates overconnectivity of short-range fiber tracts and underconnectivity of long-range tracts. Indeed, we find a decrease in global connectivity but increased local connectivity in the AgCC connectome, as shown by reduced global efficiency with increased mean local efficiency and increased mean clustering coefficient (Table 3), which may help explain why many acallosal individuals exhibit behavioral phenotypes on the autistic spectrum (Paul et al., 2007). Combined with the fact that the most common neurodevelopmental disorders have strong hereditary contributions, this supports the concept that connectomics can yield endophenotypes or "intermediate phenotypes" for genetic studies of neuropsychiatric illnesses (Fornito and Bullmore, 2012). The phenotypic

NIH-PA Author Manuscript

NIH-PA Author Manuscript

NIH-PA Author Manuscript

heterogeneity of neurodevelopmental disorders such as autism and schizophrenia, as well as their uncertain diagnostic criteria, complicate research into their genetic basis. Quantitative biomarkers derived from connectomics that capture the altered topology of whole-brain networks have the potential to identify more homogenous endophenotypes in subgroups of the patient population for hypothesis-driven tests of candidate susceptibility genes or for exploratory genome-wide association studies. The discovery and validation of connectomic intermediate phenotypes might also improve diagnosis and outcome prediction for these disorders, enabling better treatment decisions as well as better patient selection for clinical trials of experimental therapies.

Conclusions

Connectomics is a burgeoning new field that can provide novel insights into aberrant brain organization in neurodevelopmental disorders. In this initial investigation of the most common human disorder of axonal guidance, we demonstrate that the AgCC connectome has greater inter-individual variation than that of normal volunteers and also exhibits pervasive alterations in cortical and subcortical connectivity that are not limited to the absence of interhemispheric callosal fibers. Simulated lesions of these whole-brain networks yield further insights into the effect on connectivity of absent tracts like the corpus callosum and ectopic tracts such as the Probst bundles. Finally, modularity analysis was used to demonstrate that the structural core of the cerebral cortex is weakened in AgCC, primarily due to a reduction in cingulate connections. Given the growing realization that neurodevelopmental disorders are connectopathies, connectomics has the potential to revolutionize the understanding and, eventually, the diagnosis and treatment of this prevalent class of disorders.

Supplementary Material

Refer to Web version on PubMed Central for supplementary material.

Abbreviations for cortical and subcortical regions

AMG	amygdala
STS	bank of superior temporal sulcus
CAC	caudal anterior cingulate
CMF	caudal medial frontal
CAU	caudate
CUN	cuneus
ENT	entorhinal
FTP	frontal temporal pole
FUS	fusiform
HIP	hippocampus

NIH-PA Author Manuscript

NIH-PA Author Manuscript

NIH-PA Author Manuscript

IPT	inferior parietal sulcus
INS	insula
ISC	isthmus cingulate
LOC	lateral occipital
LOF	lateral orbital frontal
LIN	lingual
MOF	medial orbital frontal
MTP	medial temporal
ACB	nucleus accumbens
PRC	paracentral
PHP	pars hippocampus
POP	pars opercularis
POB	pars orbitalis
PTR	pars triangularis
PEC	pericalcarine
POC	postcentral
PCC	posterior cingulate
PRC	precentral
PCN	precuneus
PUT	putamen
RAC	rostral anterior cingulate
RMF	rostral medial frontal
SFT	superior frontal
SPT	superior parietal
STP	superior temporal
SMG	supramarginal gyrus
TPP	temporal pole
THL	thalamus
TTP	transverse temporal

References

1. Anderson BS, Butts C, Carley K. The interaction of size and density with graph level indices. Social Networks. 1999; 21:239–267.

NIH-PA Author Manuscript

NIH-PA Author Manuscript

NIH-PA Author Manuscript

2. Bassett DS, Brown JA, Deshpande V, Carlson JM, Grafton ST. Conserved and variable architecture of human white matter connectivity. Neuroimage. 2011; 54(2):1262–1279. [PubMed: 20850551]
3. Behrens TEJ, Berg HJ, Jbabdi S, Rushworth MF, Woolrich MW. Probabilistic diffusion tractography with multiple fibre orientations: What can we gain? Neuroimage. 2007; 34(1):144–155. [PubMed: 17070705]
4. Belmonte MK, Allen G, Beckel-Mitchener A, Boulanger LM, Carper RA, Webb SJ. Autism and abnormal development of brain connectivity. J Neurosci. 2004; 20(42):9228–9231. [PubMed: 15496656]
5. Blondel V, Guillame JL, Lambiotte R, Lefebvre E. Fast unfolding of communities in large networks. Journal of Statistical Mechanics: Theory and Experiment. 2008; 2008(10):P10008.
6. Bodensteiner J, Schaefer GB, Breeding L, Cowan L. Hypoplasia of the corpus callosum: a study of 445 consecutive MRI scans. J Child Neurol. 1994; 9:47–49. [PubMed: 8151082]
7. Bullmore E, Sporns O. Complex brain networks: graph theoretical analysis of structural and functional systems. Nat Rev Neurosci. 2009; 10(3):186–198. [PubMed: 19190637]
8. van Wijk BCM, Stam CJ, Daffertshofer A. Comparing Brain Networks of Different Size and Connectivity Density Using Graph Theory. PLoS ONE. 2010; 5(10):e13701. [PubMed: 21060892]
9. Engle EC. Human genetic disorders of axon guidance. Cold Spring Harb Perspect Biol. 2010; 2(3):a001784. [PubMed: 20300212]
10. Glass H, Shaw G, Ma C, Sherr EH. Agenesis of the corpus callosum in California 1983–2003: a population-based study. Am J Med Genet A. 2008; 146A:2495–2500. [PubMed: 18642362]
11. Fan Y, Shi F, Smith JK, Lin W, Gilmore JH, Shen D. Brain anatomical networks in early human brain development. NeuroImage. 2011; 54(3):1862–1871. [PubMed: 20650319]
12. Fischl B, van der Kouwe A, Destrieux C, Halgren E, Segonne F, Salat DH, Busa E, Seidman LJ, Goldstein J, Kennedy D, Caviness V, Makris N, Rosen B, Dale AM. Automatically parcellating the human cerebral cortex. Cereb Cortex. 2004; 14:11–22. [PubMed: 14654453]
13. Fornito A, Bullmore ET. Connectomic intermediate phenotypes for psychiatric disorders. Front Psychiatry. 2012; 3(32) Epub 2012 Apr 19.
14. Gong G, He Y, Concha L, Lebel C, Gross D, Evans A, Beaulieu C. Mapping Anatomical Connectivity Patterns of Human Cerebral Cortex Using In Vivo Diffusion Tensor Imaging Tractography. Cerebral Cortex. 2009; 19(3):524–536. [PubMed: 18567609]
15. Hagmann P, Kurant M, Gigandet X, Thiran P, Wedeen VJ, Meuli R, Thiran JP. Mapping Human Whole-Brain Structural Networks with Diffusion MRI. PLoS ONE. 2007; 2(7):e597. [PubMed: 17611629]
16. Hagmann P, Cammoun L, Gigandet X, Meuli R, Honey C, Wedeen V, Sporns O. Mapping the Structural Core of Human Cerebral Cortex. PLoS Biol. 2008; 6(7):e159. [PubMed: 18597554]
17. Hagmann P, Cammoun L, Gigandet X, Gerhard S, Grant PE, Wedeen V, Meuili R, Thiran JP, Honey CJ, Sporns O. MR connectomics: Principles and challenges. Journal of Neuroscience Methods. 2010; 194(1):34–45. [PubMed: 20096730]
18. Hagmann P, Grant PE, Fair DA. MR Connectomics: A Conceptual Framework for Studying The Developing Brain. Frontiers in Systems Neuroscience. 2012; 6(43)
19. Hetts SW, Sherr EH, Chao S, Gobuty S, Barkovich AJ. Anomalies of the Corpus Callosum: An MR Analysis of the Phenotypic Spectrum of Associated Malformations. American Journal of Roentgenology. 2006; 187(5):1343–1348. [PubMed: 17056927]
20. van den Heuvel MP, Sporns O. Rich-Club Organization of the Human Connectome. The Journal of Neuroscience. 2011; 31(44):15775–15786. [PubMed: 22049421]
21. Hofer S, Frahm J. Topography of the human corpus callosum revisited -Comprehensive fiber tractography using diffusion tensor magnetic resonance imaging. NeuroImage. 2006; 32(3):989–994. [PubMed: 16854598]
22. Irimia A, Chambers M, Torgerson C, Filippou M, Hovda D, Alger J, Guido G, Toga A, Vespa P, Kikinis R, Van Horn J. Patient-tailored connectomics visualization for the assessment of white matter atrophy in traumatic brain injury. Frontiers in Neurology. 2012; 3(10)
23. Iturria-Medina Y, Canales-Rodríguez EJ, Melie-García L, Valdés-Hernández PA, Martínez-Montes E, Alemán-Gómez Y, Sánchez-Bornot JM. Characterizing brain anatomical connections

NIH-PA Author Manuscript

NIH-PA Author Manuscript

NIH-PA Author Manuscript

using diffusion weighted MRI and graph theory. NeuroImage. 2007; 36(3):645–660. [PubMed: 17466539]

24. Jenkinson, M. Measuring Transformation Error by RMS Deviation. FMRIB Technical Report TR99MJ1. 1999. http://www.fmrib.ox.ac.uk/analysis/techrep/tr99mj1/tr99mj1/tr99mj1.html.
25. Jenkinson M, Bannister P, Brady M, Smith S. Improved optimization for the robust and accurate linear registration and motion correction of brain images. Neuroimage. 2002; 17:825–841. [PubMed: 12377157]
26. Jeret JS, Serur D, Wisniewski K, Fisch C. Frequency of agenesis of the corpus callosum in the developmentally disabled population as determined by computerized tomography. Pediatr Neurosci. 1985; 12:101–103. [PubMed: 2428024]
27. Kashima H, Tsuda K, Inokuchi A. Marginalized kernels between labeled graphs. 20th International Conference on Machine Learning (ICML2003). 2003
28. Khanna P, Poliakov AV, Ishak GE, Poliachik SL, Friedman SD, Saneto RP, Novotny EJ, Ojemann JG, Shaw DW. Preserved interhemispheric functional connectivity in a case of corpus callosum agenesis. Neuroradiology. 2012; 54(2):177–179. [PubMed: 21553342]
29. Kuceyeski A, Maruta J, Niogi SN, Ghajar J, Raj A. The generation and validation of white matter connectivity importance maps. NeuroImage. 2011; 58(1):109–121. [PubMed: 21722739]
30. Lee SK, Mori S, Kim DJ, Kim SY, Kim SY, Kim DI. Diffusion tensor MR imaging visualizes the altered hemispheric fiber connection in callosal dysgenesis. AJNR Am J Neuroradiol. 2004; 25:25–28. [PubMed: 14729523]
31. Lee SK, Kim DI, Kim J, Kim DJ, Kim HD, Kim DS, Mori S. Diffusion-Tensor MR imaging and fiber tractography: a new method of describing aberrant fiber connections in developmental CNS anomalies. Radiographics. 2005; 25(1):53–68. [PubMed: 15653586]
32. Li L, Rilling JK, Preuss TM, Glasser MF, Hu X. The effects of connection reconstruction method on the interregional connectivity of brain networks via diffusion tractography. Human Brain Mapping. 2012a; 33(8):1894–913. [PubMed: 21928316]
33. Li L, Rilling JK, Preuss TM, Glasser MF, Damen FW, Hu X. Quantitative assessment of a framework for creating anatomical brain networks via global tractography. Neuroimage. 2012b; 61:1017–1030. [PubMed: 22484406]
34. Li Y, Yang F, Shetty C, Venugopal S, Bukshpun P, Wakahiro M, Sherr E, Mukherjee P. Independent component analysis of resting-state fMRI reveals diminished functional connectivity in callosal dysgenesis, The 19th Annual Meeting & Exhibition of ISMRM & the 20th Annual Meeting of SMRT. Montréal, Canada. 2011
35. Lum C, McAndrews MP, Holodny AI, McManus KA, Crawley A, Chakraborty S, Mikulis DJ. Investigating Agenesis of the Corpus Callosum Using Functional MRI: A Study Examining Interhemispheric Coordination of Motor Control. Journal of Neuroimaging. 2011; 21(1):65–68. [PubMed: 19758290]
36. Meskaldji DE, Ottet M, Cammoun L, Hagmann P, Meuli R, Eliez S, Thiran JP, Morgenthaler S. Adaptive Strategy for the Statistical Analysis of Connectomes. PLoS ONE. 2011; 6(8):e23009. [PubMed: 21829681]
37. Nakata Y, Barkovich AJ, Wahl M, Strominger Z, Jeremy RJ, Wakahiro M, Mukherjee P, Sherr EH. Diffusion abnormalities and reduced volume of the ventral cingulum bundle in agenesis of the corpus callosum: a 3T imaging study. AJNR Am J Neuroradiol. 2009; 30(6):1142–1148. [PubMed: 19246528]
38. Nugent AA, Kolpak AL, Engle EC. Human disorders of axon guidance. Curr Opin Neurobiol. 2012 [Epub ahead of print].
39. Paul LK, Brown W, Adolphs R, Tyszka JM, Richards LJ, Mukherjee P, Sherr EH. Agenesis of the corpus callosum: genetic, developmental and functional aspects of connectivity. Nat Rev Neurosci. 2007; 8(4):287–299. [PubMed: 17375041]
40. Paul LK. Developmental malformation of the corpus callosum: a review of typical callosal development and examples of developmental disorders with callosal involvement. J Neurodev Disord. 2011; 3(1):3–27. [PubMed: 21484594]

NIH-PA Author Manuscript

NIH-PA Author Manuscript

NIH-PA Author Manuscript

41. Ren T, Zhang J, Plachez C, Mori S, Richards LJ. Diffusion tensor magnetic resonance imaging and tract-tracing analysis of Probst bundle structure in Netrin1- and DCC-deficient mice. J Neurosci. 2007; 27(39):10345–9. [PubMed: 17898206]
42. Rubinov M, Sporns O. Complex network measures of brain connectivity: Uses and interpretations. NeuroImage. 2010; 52(3):1059–1069. [PubMed: 19819337]
43. Seung, S. Connectome: How the Brain's Wiring Makes Us Who We Are. New York, NY: Houghton Mifflin Harcourt; 2012.
44. Shu N, Liu Y, Li J, Yonghui L, Chunshui Y, Jiang T. Altered Anatomical Network in Early Blindness Revealed by Diffusion Tensor Tractography. PLoS ONE. 2009; 4(9):e7228. [PubMed: 19784379]
45. Smith S. Fast robust automated brain extraction. Human Brain Mapp. 2002; 17:143–155.
46. Sporns O, Tononi G, Kotter R. The Human Connectome: A Structural Description of the Human Brain. PLoS Comput Biol. 2005; 1(4):e42. [PubMed: 16201007]
47. Sporns O. The human connectome: a complex network. Annals of the New York Academy of Sciences. 2011; 1224(1):109–125. [PubMed: 21251014]
48. Tovar-Moll F, et al. Neuroplasticity in Human Callosal Dysgenesis: A Diffusion Tensor Imaging Study. Cerebral Cortex. 2007; 17(3):531–541. [PubMed: 16627861]
49. Tymofiyeva O, Hess C, Ziv E, Tian N, Bonifacio S, McQuillen P, Ferriero D, Barkovich J, Xu D. Towards the Baby Connectome: Mapping the Structural Connectivity of the Newborn Brain. PLoS ONE. 2012; 7(2):e31029. [PubMed: 22347423]
50. Tyszka JM, Kennedy DP, Adolphs R, Paul LK. Intact Bilateral Resting-State Networks in the Absence of the Corpus Callosum. The Journal of Neuroscience. 2011; 31(42):15154–15162. [PubMed: 22016549]
51. Vaessen MJ, Hofman PA, Tijssen HN, Aldenkamp AP, Jansen JF, Backes WH. The effect and reproducibility of different clinical DTI gradient sets on small world brain connectivity measures. Neuroimage. 2010; 51(3):1106–1116. [PubMed: 20226864]
52. Verstraete E, Veldink JH, Mandl RCW, van den Berg LH, van den Heuvel MP. Impaired Structural Motor Connectome in Amyotrophic Lateral Sclerosis. PLoS ONE. 2011; 6(9):e24239. [PubMed: 21912680]
53. Vishwanathan SVN, Schraudolph NN, Kondor R, Borgwardt KN. Graph kernels. J Machine Learning Research. 2010; 11:1201–1242.
54. Wahl M, Strominger Z, Jeremy RJ, Barkovich AJ, Wakahiro M, Sherr EH, Mukherjee P. Variability of Homotopic and Heterotopic Callosal Connectivity in Partial Agenesis of the Corpus Callosum: A 3T Diffusion Tensor Imaging and Q-Ball Tractography Study. American Journal of Neuroradiology. 2009; 30(2):282–289. [PubMed: 19001538]
55. Wahl M, Barkovich AJ, Mukherjee P. Diffusion imaging and tractography of congenital brain malformations. Pediatric Radiology. 2010; 40(1):59–67. [PubMed: 19937239]
56. Wang LW, Huang CC, Yeh TF. Major brain lesions detected on sonographic screening of apparently normal term neonates. Neuroradiology. 2004; 46:368–73. [PubMed: 15103432]
57. Yan C, Gong G, Wang J, Wang D, Liu D, Zhu C, Chen ZJ, Evans A, Zang Y, He Y. Sex- and Brain Size-Related Small-World Structural Cortical Networks in Young Adults: A DTI Tractography Study. Cerebral Cortex. 2011; 21(2):449–458. [PubMed: 20562318]
58. Yap P-T, Fan Y, Chen Y, Gilmore JH, Lin W, Shen D. Development Trends of White Matter Connectivity in the First Years of Life. PLoS ONE. 2011; 6(9):e24678. [PubMed: 21966364]

NIH-PA Author Manuscript
NIH-PA Author Manuscript
NIH-PA Author Manuscript

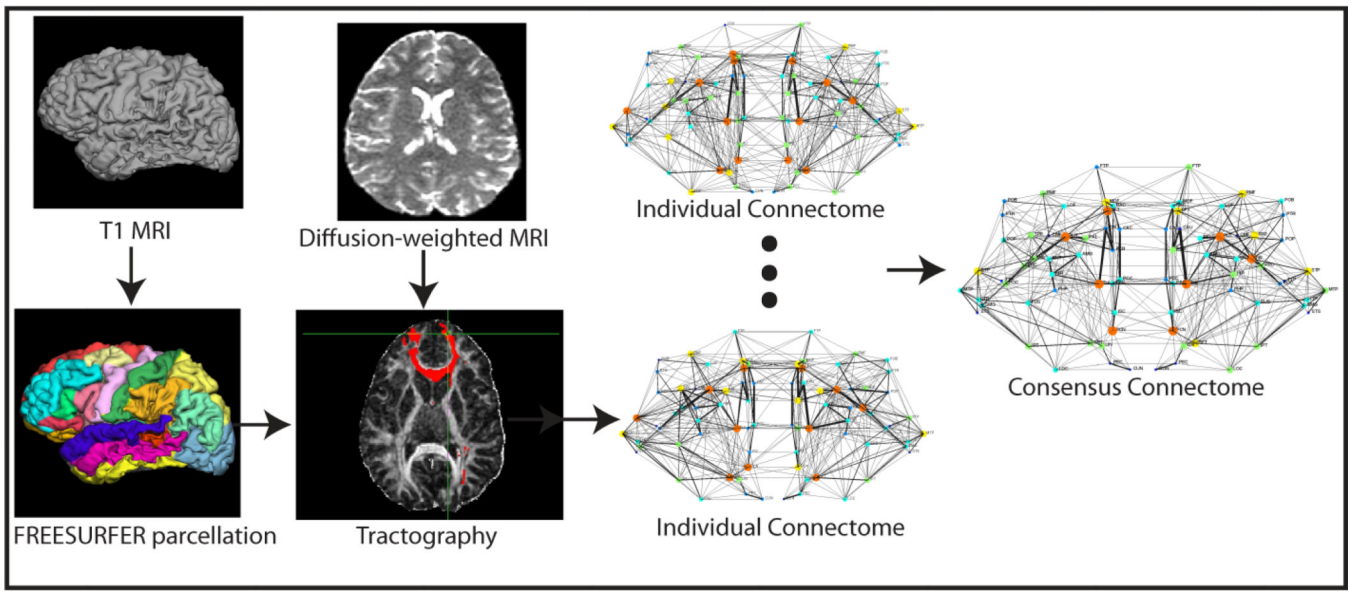

Figure 1.

The connectome processing pipeline utilized in this paper. FreeSurfer was used to parcellate the T1 MRI and FSL's probtrackx2 was used to perform probabilistic tractography. The individual connectomes were combined to create a consensus connectome for each group.

NIH-PA Author Manuscript
NIH-PA Author Manuscript
NIH-PA Author Manuscript

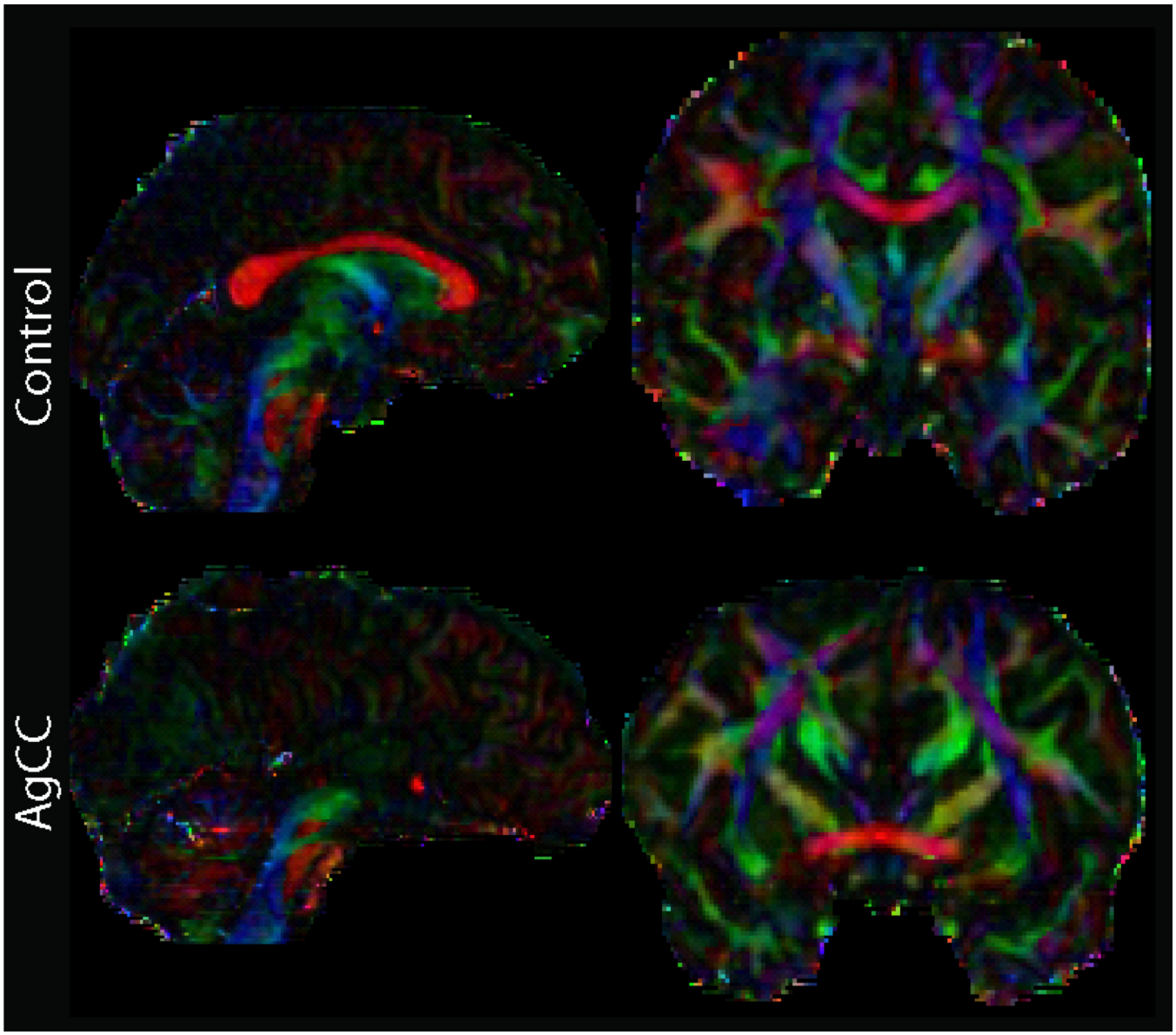

Figure 2.
Example midline sagittal and coronal color fractional anisotropy (FA) images for a control subject (*top row*) and an AgCC subject (*bottom row*).

NIH-PA Author Manuscript
NIH-PA Author Manuscript
NIH-PA Author Manuscript

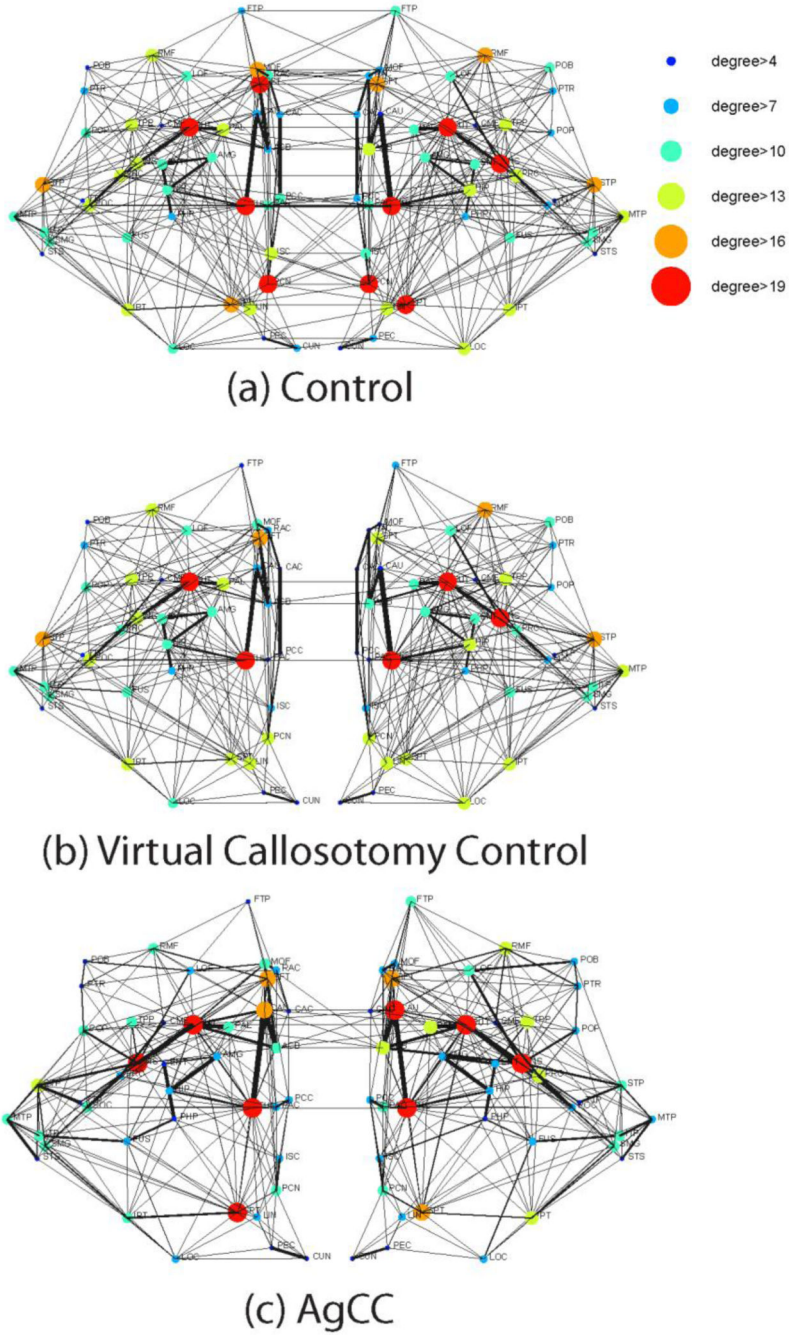

Figure 3.

Consensus connectomes for the *a*) control group, *b*) controls after virtual callosotomy, and *c*) AgCC group. The connectomes are displayed in the neurological convention and anterior is up and posterior is down. The 82 nodes are plotted with a circle scaled and colored according to the degree of the node (*legend*). A line between two nodes represents a suprathreshold connection, where the weight of the lines scales with the strength, although unweighted connectomes were used for the degree calculation.

NIH-PA Author Manuscript

NIH-PA Author Manuscript

NIH-PA Author Manuscript

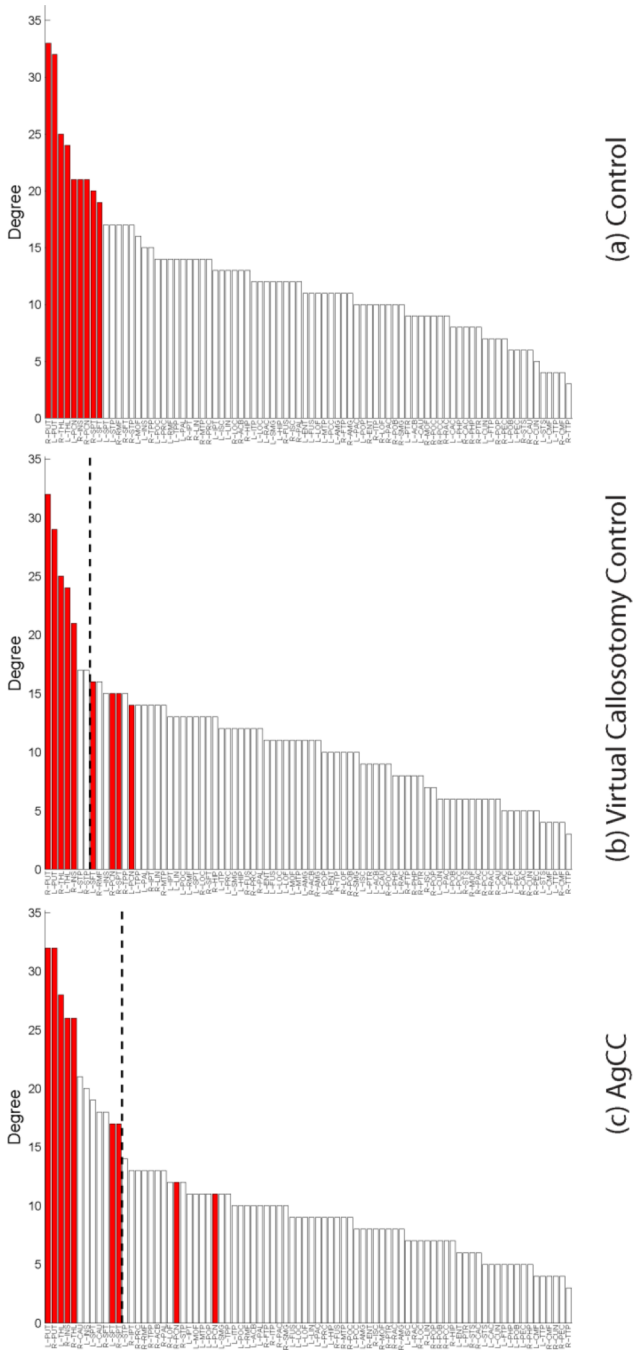

Figure 4.

Degree distribution across nodes for the consensus connectomes. The bars in red demonstrate the nodes with degree greater than mean plus one standard deviation for the control consensus connectome in (*a*). The dotted lines in (*b*) and (*c*) demonstrate the cutoff for mean plus one standard deviation in the virtual callostomy controls and AgCC. The red bars in (*b*) and (*c*) show the redistribution of regions in the virtual callostomy and AgCC consensus connectomes, respectively, that are hubs in the control consensus connectome.

NIH-PA Author Manuscript

NIH-PA Author Manuscript

NIH-PA Author Manuscript

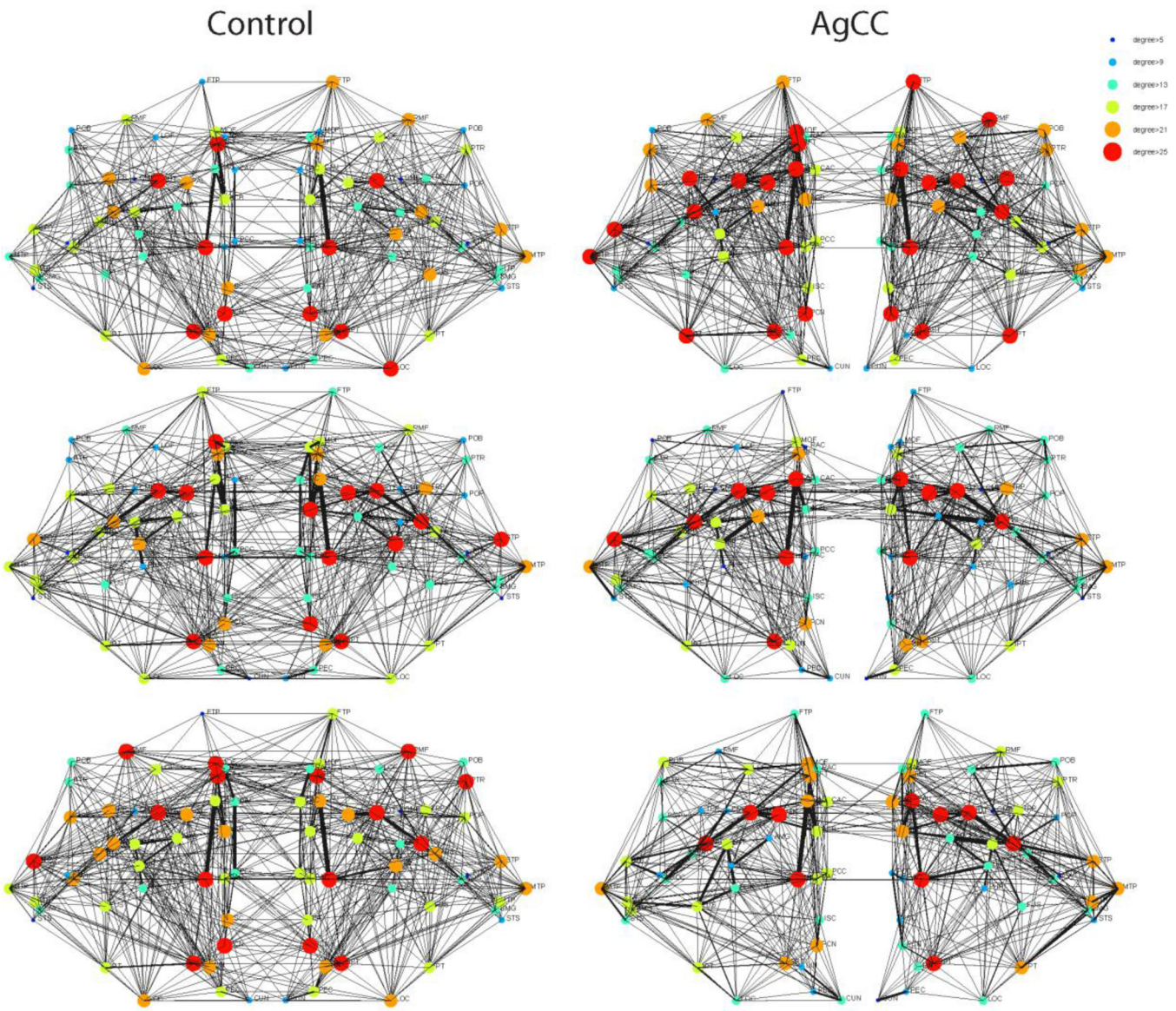

Figure 5.

Three example individual connectomes for the controls (*left*) and for AgCC (*right*). The connectomes are displayed in the neurological convention and anterior is up and posterior is down. The 82 nodes are plotted with a circle scaled and colored according to the degree of the node (see legend). A line between two nodes represents a suprathreshold connection, where the weight of the lines scales with the strength, but unweighted connectomes were used for the degree calculation. The controls exhibit some variability, but the overall distribution of degree is constant. The AgCC connectomes demonstrate more variability in the location and number of hub regions.

NIH-PA Author Manuscript

NIH-PA Author Manuscript

NIH-PA Author Manuscript

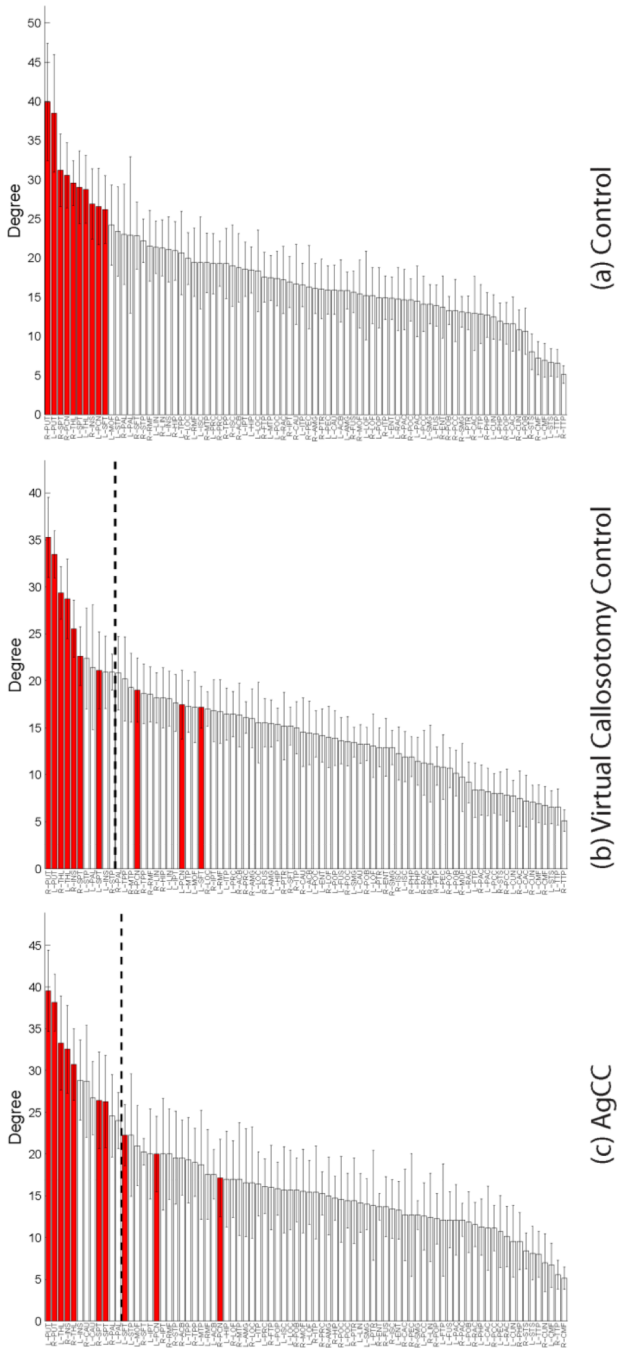

Figure 6.

Mean degree distribution across nodes for the individual connectomes with standard deviation error bars. The bars colored red demonstrate the nodes with degree greater than mean plus one standard deviation for the controls. The dotted lines in (*b*) and (*c*) demonstrate the cutoff for mean plus one standard deviation for the virtual callostomy controls and for AgCC, respectively. The red bars in (*b*) and (*c*) show the redistribution of regions in the individual connectomes of the virtual callostomy and AgCC groups, respectively, that are hubs in the individual connectomes of the control subjects.

NIH-PA Author Manuscript
NIH-PA Author Manuscript
NIH-PA Author Manuscript

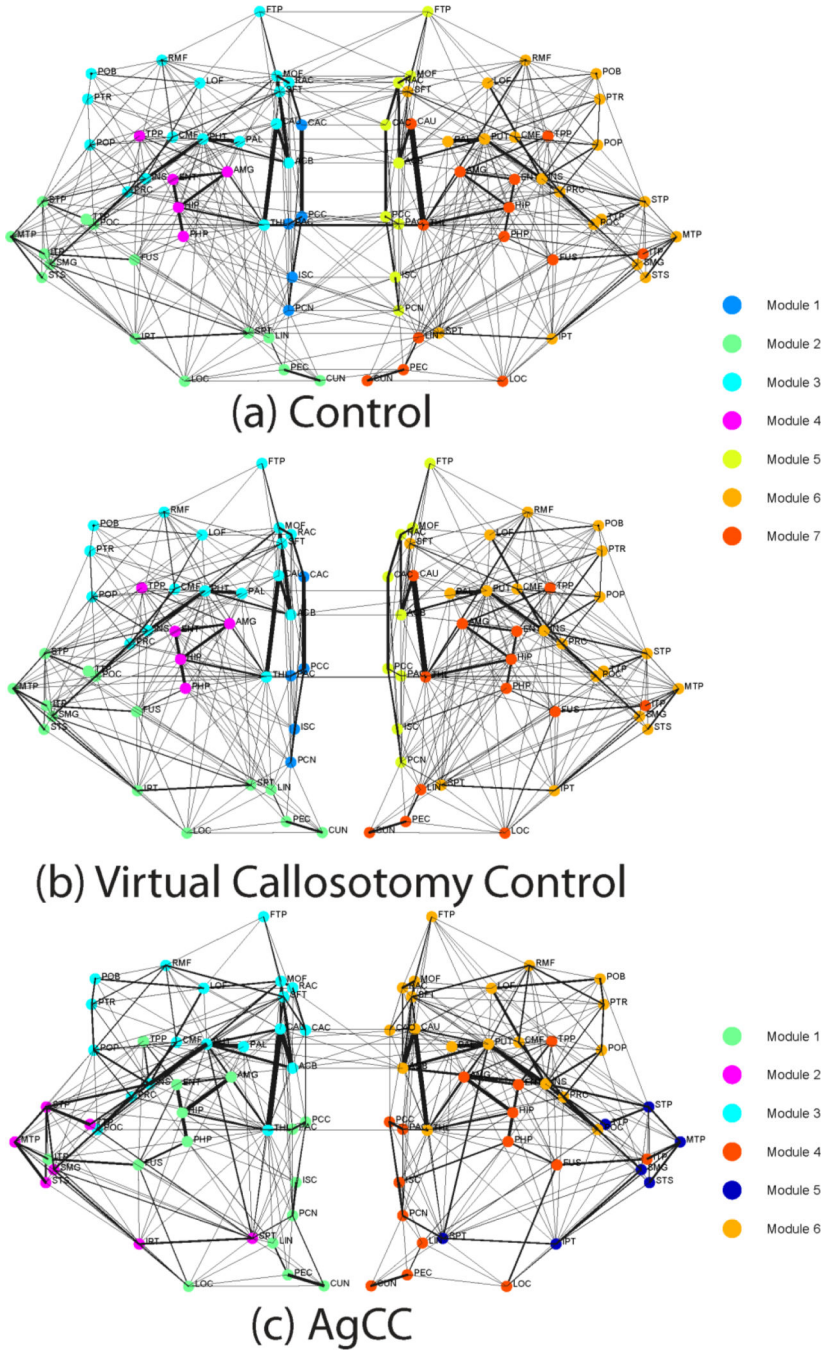

Figure 7.

The module assignments for the consensus connectomes. The connectomes are displayed in the neurological convention and anterior is up and posterior is down. The 82 nodes are plotted with a circle colored according to the community to which it was assigned (*legend*). A line between two nodes represents a suprathreshold connection, where the weight of the lines scales with the strength. The weighted connectomes were used for modularity analysis.

NIH-PA Author Manuscript

NIH-PA Author Manuscript

NIH-PA Author Manuscript

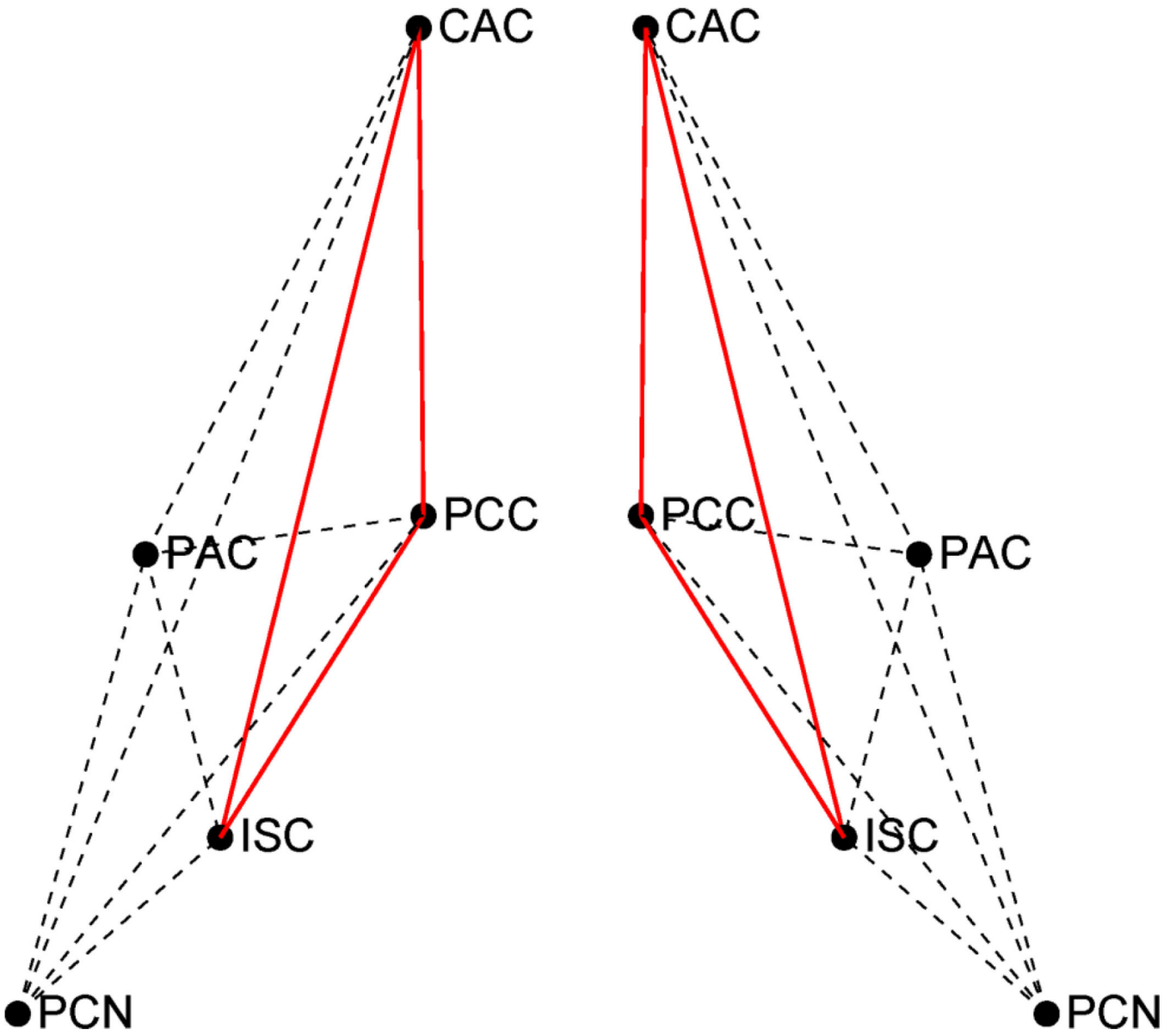

Figure 8.

The medial cortical modules ("structural core") as identified in the control consensus connectome. The edges colored red were significantly weaker in the AgCC group compared to the controls at $p<0.05$, corrected for multiple comparisons using the false discovery rate.

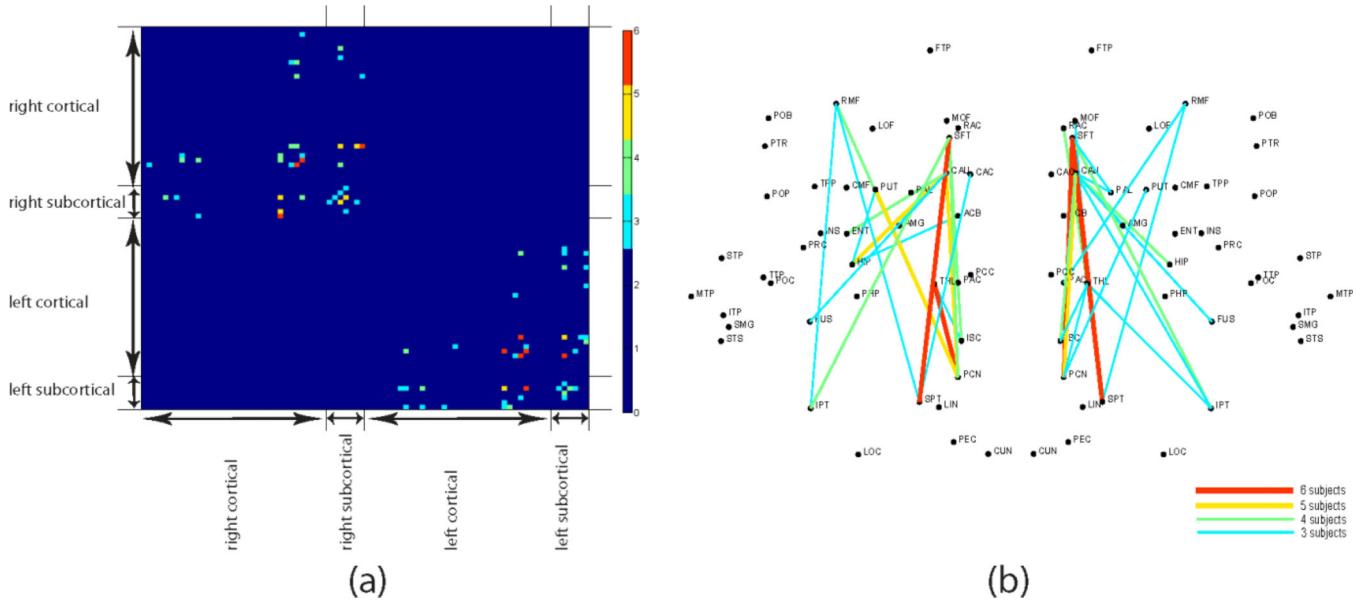

Figure 9.

The virtual Probstotomy results show that excluding the Probst bundle fibers reliably affects the corticocortical connections, as well as cortical-subcortical and subcortical-subcortical connections. Figure 9 (a) plots the number of subjects for which each pair-wise connection strength was reduced. Reduced connections were defined as those with percent differences in connection strength, before and after the Probstotomy, greater than the mean plus one standard deviation. Figure 9(b) displays the connections where at least three of seven subjects showed reduced connection strengths after the Probstotomy.

NIH-PA Author Manuscript
NIH-PA Author Manuscript
NIH-PA Author Manuscript

NIH-PA Author Manuscript

NIH-PA Author Manuscript

NIH-PA Author Manuscript

Table 1

Unweighted Network Metrics of Consensus Connectomes

Network Metric	Control	Virtual Callosotomy	AgCC
Mean degree	12.1	10.9	10.6
Cost	0.15	0.13	0.13
Characteristic path length	2.26	2.60	2.50
Mean normalized betweenness	0.032	0.041	0.038
Global efficiency	0.50	0.46	0.47
Mean local efficiency	0.77	0.80	0.80
Mean clustering coefficient	0.56	0.61	0.61

NIH-PA Author Manuscript

NIH-PA Author Manuscript

NIH-PA Author Manuscript

Table 2

Network Consistency (correlation coefficient of connection strengths)

	Control	Virtual Callosotomy	AgCC
Consistency of individual networks with the consensus network	0.926±0.014	0.928±0.012	0.912±0.048
Consistency between individual networks	0.846±0.034	0.850±0.030*	0.808±0.042*

*denotes significantly different from Control group ($p<0.05$)

The significant difference detected in the consistency between individual networks for the Control and Virtual Callosotomy groups is driven, in part, by differing distributions of these values. Even though the mean plus one standard deviation would indicate these values overlap, the virtual callosotomy distribution has a heavier tail than the control distribution.

NIH-PA Author Manuscript

NIH-PA Author Manuscript

NIH-PA Author Manuscript

Table 3

Unweighted Network Metrics of Individual Connectomes (average ± std deviation)

Network Metric	Control	Virtual Callosotomy	AgCC
Mean degree	17.7±2.2	14.9±1.5*	16.7±2.6
Cost	0.22±0.03	0.18±0.02*	0.21±0.03
Characteristic path length	1.98±0.09	2.36±0.09*	2.21±0.10*
Mean normalized betweenness	0.025±0.002	0.035±0.002*	0.031±0.002*
Global efficiency	0.57±0.03	0.51±0.02*	0.53±0.03*
Mean local efficiency	0.79±0.01	0.81±0.01*	0.83±0.03*
Mean clustering coefficient	0.59±0.02	0.64±0.02*	0.67±0.04*

* denotes significantly different from Control group ($p<0.05$)

NIH-PA Author Manuscript

NIH-PA Author Manuscript

NIH-PA Author Manuscript

Table 4

Modularity Metrics

Modularity Metrics	Control	Virtual Callosotomy	AgCC
Mean modularity (individual connectomes)	0.58±0.02	0.60±0.01*	0.59±0.04
Mean participation coefficient (individual connectomes)	0.35±0.03	0.28±0.03*	0.25±0.05*
Hubert rand index (compared to consensus partition)	0.79±0.06	0.79±0.06	0.74±0.08*
Hubert rand index (compared to individual partition)	0.742±0.057	0.739±0.063*	0.69±0.060*

*denotes significantly different from Control group ($p<0.05$)